



LUMINOUS RED GALAXIES IN SIMULATIONS



A thesis submitted in partial fulfilment of the requirements
for the degree of Master in Astrophysics in the Department
of Physics, University of Western Cape.

Supervisor : Prof Catherine Cress

Co-supervisor : Dr Enrico Olivier

March 2010

LUMINOUS RED GALAXIES IN SIMULATIONS

ANDO LALAINA RATSIMBAZAFY

KEYWORDS :

Cosmology parameters

Early-type Galaxies

Galaxy abundances

Galaxy Evolution

Galaxies

Luminous Red Galaxies

Millenium Simulation

Observational cosmology

Semi-analytical model

Universe



Abstract

LUMINOUS RED GALAXIES IN SIMULATIONS

A.L.Ratsimbazafy

MSc Thesis, Department of Physics, University of Western Cape.

There have been a number of attempts to measure the expansion rate of the Universe using age-dating of Luminous Red Galaxies (LRGs). Assuming stars in LRGs form at the same time, age-dating of two populations of LRGs at different redshifts can provide an estimate of the time difference associated with the corresponding redshift interval (dt/dz). This gives a direct estimate of the Hubble parameter at the average redshift of the two populations. In this thesis, we explore the validity of the assumptions in this method using LRGs identified in the Millenium Simulation. We study the properties of LRGs simulated using two semi-analytical models for galaxy evolution and discuss LRG selection criteria. We use stellar population modelling and spectral synthesis to estimate the errors on ages that can be expected and discuss optimization of an age-dating experiment. We find that $H(z)$ using simulated galaxies from MS can be recovered with high accuracy. Using Single Stellar Populations (SSPs) to age -date LRGs is not sufficient for this experiment but if the star formation histories of galaxies are used, accurate ages are obtainable. We discuss an observing program to carry out this experiment using SALT (Southern African Large Telescope).

March 2010

DECLARATION

I declare that *Luminous Red Galaxies in Simulations* is my own work as well as the outcome of scientific collaborations stated below, that it has not been submitted before for any degree or examination in any other University. The content of this thesis includes work presented in the following research paper (submitted to the Journal: Monthly Notices of the Royal Astronomical Society) and that sources I have used or quoted have been indicated and acknowledged as complete references.

Paper:

”Luminous Red Galaxies in Simulations: Cosmic Chronometers?”

S. M. Crawford, **A. L. Ratsimbazafy**, C. M. Cress, E. A. Olivier, S-L. Blyth, K. J. van der Heyden

Monthly Notices of the Royal Astronomical Society (MNRAS), 2009 submitted



Ando Lalaina Ratsimbazafy

March 2010

Signed :

List of Figures

- 1 Hierarchical galaxy formation simplified by neglecting the "subhalo" concept. 20
- 2 The sky coverage of the SDSS imaging survey. Credit from the Sloan Digital Sky Survey website (www.sdss.org) 28
- 3 The distribution of the SDSS LRG and 2SLAQ catalogues. **Black points:** main galaxies from the SDSS-data release 3 (SDSS-DR3); **red points:** main galaxies from the 2SLAQ; **green points:** LRGs from the SDSS-DR3; **blue points:** LRGs from the 2SLAQ. Credit from the 2SLAQ website (www.2slaq.info) 29
- 4 The effect of varying the brightness cut (top panel) and the colour cut (bottom panel) on the mass-weighted age histogram for galaxies at $z = 0.51$. Sample extracted from the de Lucia et al. model. 31
- 5 The average SFR using SDSS and absolute magnitude cuts in **upper panel:** the de Lucia et al. model; and **bottom panel:** the Bower et al. model. Black lines represent the average SFR at $z = 0.32$; green at $z = 0.46$; blue at $z = 0.51$ and red at $z = 0.56$ 39
- 6 The star formation history for 50 randomly selected model galaxies in the de Lucia et al. model at $z = 0.32$ 40
- 7 The ratio of the average star formation histories in figure 6 to the average star formation history for the $z = 0.32$ sample. Black lines represent the average SFR at $z = 0.32$; green at $z = 0.46$; blue at $z = 0.51$ and red at $z = 0.56$ 41
- 8 Histogram of the mass-weighted ages at four different redshifts in the two models using the two cuts. Black lines represent the average SFR at $z = 0.32$; green at $z = 0.46$; blue at $z = 0.51$ and red at $z = 0.56$ 43
- 9 Metallicity distribution of LRGs at four different redshifts in the two models using the two cuts. Black filled dots represent the average SFR at $z = 0.32$; green stars at $z = 0.46$; blue diamonds at $z = 0.51$ and red squares at $z = 0.56$. *Notes:* in the de Lucia et al. model, we extracted the metallicity of the cold gas out of which LRGs are formed, however in the Bower et al. model, we extracted the luminosity weighted metallicity. 50

10	Stellar masses distribution of LRGs at four different redshifts in the two models using the two cuts. Black filled dots represent the average SFR at $z = 0.32$; green stars at $z = 0.46$; blue diamonds at $z = 0.51$ and red squares at $z = 0.56$	52
11	Distribution of dark halo masses hosting LRGs at four different redshifts in the two models using the two cuts. Black filled dots represent the average SFR at $z = 0.32$; green stars at $z = 0.46$; blue diamonds at $z = 0.51$ and red squares at $z = 0.56$	53
12	Colour distribution of LRGs at four different redshifts in the two models using the two cuts. Black filled dots represent the average SFR at $z = 0.32$; green stars at $z = 0.46$; blue diamonds at $z = 0.51$ and red squares at $z = 0.56$	54
13	The predicted morphological mix of LRGs in the two models at four different redshift bins. Red dashed lines represent galaxies from the de Lucia et al. model, whereas blue solide lines from Bower et al. model using the absolute magnitude cuts. f is the number of galaxies normalized.	55
14	The difference between $H(z)$ and $\frac{\Delta z}{\Delta t}$ calculated from the Average (top), Fixed fit (middle), and Pair 20 (bottom) methods. The size of each point is related to the distance between the redshift snapshots which range from $\Delta z = 0.02 - 0.91$. Larger errors are typically associated with smaller redshifts intervals.	61
15	Average spectrum of 200 SDSS LRGs from galaxies at $z = 0.46$ satisfying the absolute magnitude cuts, compared to the best-fit model spectrum produced using the BC03 model with the SFH and metallicity from the MS at $z = 0.46$. The spectrum is normalized to observed values at 4130 \AA	67
16	The average systematic offset between the model age and the mass-weighted age as a function of SNR and resolution for 10 different galaxies (Top panel). Random error in the age determination for the same 10 galaxies (bottom panel).	69
17	The uncertainty in the mean age of LRGs at $z = 0.51$ as a function of the number of galaxies used for the measurement. We assumed four different uncertainties ($0.05, 0.50, 1, 2Gyr$) in the measured age of an individual galaxy in sample	74

- 18 The total observing time required with SALT to measure $H(z)$ at $z \approx 0.415$ to 3, 5 and 10% as a function of SNR of the observations. All observations are for $\Delta\lambda = 3 \text{ \AA}$ and an overhead of 300 s per observation. 75



List of Tables

1	The cosmological parameters deduced from different type of data . . .	9
2	Number of objects using the two different selection criteria extracted from the two catalogues.	34
3	The space density of LRGs predicted by the two models using the SDSS and absolute magnitude cuts compared with the space density of observed LRG-like objects extracted from SDSS database using our absolute magnitude cuts.	35
4	Formation properties of LRGs	37
5	The comparison between the change of the average mass-weighted age of the LRGs and the change of the age of the Universe Age^a	44
6	The stellar masses range and its median for each redshift bin in the models.	51
7	The predicted morphological mix of LRGs at different redshifts in the two models.	56
8	Errors from age-dating. Comparison between ages and errors in ages from SSP fitting and from fitting with our model spectra.	68

WESTERN CAPE

Acknowledgments

I would like to thank my supervisor Prof Catherine Cress, for her invaluable guidance and enthusiasm during this project. I am grateful to the Virgo Consortium team (Millenium Simulation), in particular Gerard Lemson, for allowing me to access to their data.

I wish to extend special thanks to the SCALPEL team, in particular Dr Enrico Olivier who was my co-supervisor, for their invaluable suggestions and theoretical input.

I acknowledge funding from the South Africa Square Kilometre Array (SA SKA) and the Centre for High Performance Computing (CHPC).

Finally, I would like to give special thanks to all those who gave me support, friendship and love, but let me mention especially my Parents, my brother, my sister, and Andry Rajoelimanana.



Contents

Title	i
Abstract	i
Declaration	ii
Acknowledgments	iii
List of figures	iii
List of tables	iii
1 Introduction	1
1.1 Overview	2
1.2 The Standard cosmological model and galaxy evolution	4
1.3 LRGs background	11
1.4 Simulation characteristics	13
2 Semi-analytical models for galaxy evolution: two models	15
2.1 Gas cooling, star formation and supernova feedback	17
2.2 Mergers and disk instability	19
2.3 Black holes and AGN feedback	23
3 Identifying LRGs	26
3.1 The Millenium Run database	27
3.2 LRGs selection criteria	27
4 Properties of LRGs	32
4.1 The abundance of LRGs	33
4.2 Star formation history of LRGs	35
4.2.1 Results in the de Lucia et al. model	36
4.2.2 Results in the Bower et al. model	38

4.3	The distribution of ages of stellar populations and metallicity	42
4.4	Stellar mass	46
4.5	Dark halo mass	47
4.6	Colours of simulated LRGs	48
4.7	Morphology of LRGs	48
4.8	Summary	56
5	Recovering $H(z)$	58
5.1	Method	59
5.2	Results	60
6	Simulated Spectra of LRGs	63
6.1	Stellar population synthesis models	65
6.2	Modelling LRG spectra	66
6.3	Age-dating simulated LRG spectra with SSPs	67
6.4	Age-dating simulated LRG spectra with model spectra	70
6.5	Summary	70
7	Observation constraints	72
8	Summary and Conclusion	77
8.1	Summary	78
8.2	Outlook	80
	Bibliography	81

Chapter 1

1 Introduction



1.1 Overview

Almost eighty years ago, Edwin Hubble measured the expansion rate of the Universe with his pioneering observations of galaxies (Hubble, 1936). Since then galaxies have been important tools for understanding the structure and evolution of the Universe. The expansion rate of the Universe has been measured locally (Freedman et al., 2001) but is not well measured at high redshifts. A method to constrain this parameter is described by Jimenez and Loeb (2002) using age-dating of stellar populations of Luminous Red galaxies (LRGs). Measuring directly $H(z)$ can provide a more direct constraint on cosmological parameters (Jimenez and Loeb, 2002).

This project forms part of the larger SCALPEL project (SALT Cosmic Ages of Luminous Passives Ellipticals Survey), which aims to constrain the expansion rate of the universe at a redshift of $z \approx 0.5$ to within 10% using LRGs observed with SALT. By measuring the age difference between two ensembles of passively-evolving galaxies at somewhat different redshifts, one can calculate the Hubble constant $H(z)$ at high redshifts using the derivative of cosmic time with respect to redshift interval dt/dz . Using a similar method, Jimenez et al. (2003) measured the Hubble parameter today, obtaining $H_0 = 69 \pm 12 \text{ km s}^{-1} \text{ Mpc}^{-1}$ with the SDSS (Sloan Digital Sky Survey) data. Apart from that, a number of scientists have attempted to use this method (e.g Ferreras et al., 2001; Capozziello et al., 2004; Ferreras et al., 2003; Simon et al., 2005; Dantas et al., 2007; Verkhodanov et al., 2005; Samushia et al., 2009) to track the evolution of $H(z)$ as a function of redshift, and place constraints on cosmological parameters.

Here, we use large N-body simulations in combination with semi-analytical models for galaxy evolution to simulate the properties of LRGs that will be used for these "cosmic chronometers". We are using these simulations to study the predictions that "standard" galaxy evolution models make for LRGs and to optimize the SCALPEL experiment. In particular, we are investigating the optimal redshift, redshift interval, number of LRGs and spectroscopic signal-to-noise ratio required for the experiment. We attempt to compare the predictions from two published models using different se-

lection criteria. One of the models has successfully reproduced many observations of elliptical galaxies, (De Lucia et al., 2006), (one of the MPA model) and the other which reproduces well the calculation of the volume averaged star formation rate density of the Universe as a function of redshift; the luminosity function; colour distribution and stellar mass functions of galaxies in the local Universe (Bower et al., 2006), (one of the Durham model). Both models consider the mechanisms to suppress the formation of massive galaxies by applying active galactic nuclei (AGN) feedback to quench cooling flows in massive haloes. Almeida et al. (2008) showed the Bower et al. model reproduces the luminosity function and the clustering of LRGs well. The parameters of the Bower et al. (2006) model also reproduce the luminosity, colour and morphology of local massive elliptical galaxies that would include LRGs.

Assuming that semi-analytical models provide appropriate star formation histories (SFHs), we optimize the selection of LRGs to obtain galaxies which match the requirements for $H(z)$ measurements. We then examine how well $H(z)$ can be recovered using the mass-weighted age of these galaxies. In addition, we carry out an initial method of age-dating that utilizes the stellar population models of Bruzual and Charlot (2003) (hereafter BC03) to synthesize spectra, and its implication for measuring $H(z)$.

The thesis is summarized as follows: in this chapter, I give an overview of the “standard” cosmological model of the Universe and provide background on galaxy evolution studies, focussing on LRGs. I also give an overview of the semi-analytical models in the Millennium simulation, which we use for this study in chapter 2. In chapter 3, I discuss selection criteria for LRGs, and in chapter 4, I investigate the properties of LRGs selected from the simulation. In chapter 5, I investigate how well $H(z)$ is recovered in the MS using LRG mass weighted ages. In chapter 6, I describe how we model the LRG spectra and age-date them. In chapter 7, I discuss an observational program to measure the $H(z)$, and I conclude in chapter 8.

1.2 The Standard cosmological model and galaxy evolution

All modern cosmological models are based on the Einstein's General Theory of Relativity (1915). The spacetime of the Universe can be described by solving Einstein's general relativistic field equations defined as

$$G_{\mu\nu} = \frac{8\pi G}{c^4} T_{\mu\nu}, \quad (1)$$

where $G_{\mu\nu}$ is the *Einstein tensor*, describing the geometry of the spacetime and $T_{\mu\nu}$ is the sum of the stress-energy tensors for the various components of energy, baryons, radiation, neutrinos, dark matter and possibly others. Since on the largest scales ($> 100Mpc$) the universe appears homogenous and there are no observations that seem to pick out preferred directions, we can model the Universe as homogenous and expanding isotropically (the same in all directions). Under these assumptions, the geometry of the Universe is greatly simplified and described by the Robertson-Walker metric:

$$ds^2 = (cdt)^2 - R^2(t) \left[\frac{dr^2}{1 - kr^2} + (rd\theta)^2 + (rsin\theta d\varphi)^2 \right], \quad (2)$$

where k describes the curvature of the space which can be *closed* ($k > 0$), *flat* ($k = 0$) or *open* ($k < 0$). This can be written in tensor notation as

$$ds^2 = g_{\mu\nu} dx^\mu dx^\nu, \quad (3)$$

where the nonvanishing components are

$$g_{00} = 1, \quad g_{11} = -\frac{R^2}{1 - kr^2}, \quad g_{22} = -R^2 r^2, \quad g_{33} = -R^2 r^2 \sin^2 \theta. \quad (4)$$

Values of $g_{\mu\nu}$ and their derivatives give the 16 components of $G_{\mu\nu}$ on the left hand side of the Einstein's field equations. We obtain:

$$G_{00} = 3(cR)^{-2}(\dot{R} + kc^2), \quad G_{11} = -c^{-2}(2R\ddot{R} + \dot{R}^2 + kc^2)(1 - kr^2)^{-1}. \quad (5)$$

On the right hand side of the Einstein's field equations, the stress energy tensor is given by

$$T_{\mu\nu} = (p + \rho c^2) \frac{v_\mu v_\nu}{c^2} - pg_{\mu\nu}, \quad (6)$$

with off-diagonal elements being zero. The four components will be

$$T_{00} = T_{11} = T_{22} = T_{33} = \frac{pR^2}{1 - kr^2}. \quad (7)$$

We note that ρc^2 is the energy density and ρ the mass density of the various components of the universe. where $R(t)$ is the cosmic scale factor. After substituting equations 5 and 6 into Einstein's equations 1, we obtain the Friedmann's equations:

$$\frac{\dot{R}^2 + kc^2}{R^2} = \frac{8\pi G}{3}\rho, \quad (8)$$

$$2\frac{\ddot{R}}{R} + \frac{\dot{R}^2 + kc^2}{R^2} = -\frac{8\pi G}{c^2}p. \quad (9)$$

The first equation (equation 8) describes a direct connection between the mass densities in the Universe and the expansion rate \dot{R} ; the second equation (equation 9) shows that it may accelerate. From equations 8 and 9, we obtain:

$$2\frac{\ddot{R}}{R} = -\frac{8\pi G}{3c^2}(\rho c^2 + 3p), \quad (10)$$

which demonstrates that the acceleration decreases with increasing pressure and energy densities. Again ρ is the mass density and p the pressure. Given an equation of state, we can solve the above equations. Since the Universe is approximated to be an ideal perfect fluid, the equation of state is given by:

$$p = \omega\rho c^2, \quad (11)$$

where the parameter ω is a constant which lies in the range $0 < \omega < 1$. There are three main cases:

- $\omega = 0 \rightarrow p = 0$ dust Universe, *matter* dominated
- $\omega = \frac{1}{3} \rightarrow p = \frac{1}{3}\rho c^2$ radiative Universe, *radiation* dominated
- $\omega = -1 \rightarrow p = -\rho c^2$ De Sitter Universe, *vacuum* dominated

We note that the Hubble parameter is defined as $H = \frac{\dot{R}}{R}$. These simplest solutions to the Einstein equations are known as Friedmann (FRW) cosmology models.

The fate of the Universe depends on the value of ρ ; in a matter dominated Universe for a given rate of expansion, there is a critical density making the comoving part of the metric look Euclidean :

$$\rho_c = \frac{3H^2}{8\pi G} \quad (12)$$

if ρ_0 exceeds this critical density, the Universe will be “*spatially closed*” and bound, i.e the Universe will collapse back towards a final “*Big Crunch*”; on the other hand, a lower density Universe will be “*spatially open*” or unbound. If ρ_0 is exactly equal to this critical density, the Universe will just expand forever (the “*critical*” or “*Einstein-de Sitter*” model), but its expansion velocity will tend asymptotically toward zero. The Universe cannot collapse at early times due to entropy production and the associated high radiation pressure.

The Universe is full of matter and the attractive force of gravity pulls all matter together. In the early 1990’s, it was believed that the expansion rate would decrease as time went on. The recent observations of high redshift supernovae Ia showed that the expansion of the Universe was actually accelerating and it has not been slowing. The existence of an exotic component called “*dark energy*”, besides ordinary matter and radiation, is the most popular way to explain this accelerating Universe. Evidence for the increasing expansion rate comes from supernova observations (Perlmutter, 1999), and other indicators such the absolute ages of high redshift galaxies (Spinrad et al., 1997), the value of Hubble constant H_0 (Freedman et al., 2001), the power spectrum of the cosmic microwave background (CMB) (Benoît, 2003) in combination with galaxy surveys (Efstathiou, 2002) and lensing (Wang et al., 2003) in addition the recent results from the *Wilkinson Microwave Anisotropy Probe* (WMAP) data (Spergel et al., 2003), all indicate that the Universe has a flat geometry and is dominated by some dark energy with negative pressure.

The nature of the dark energy component remains unclear but it is known to be very homogeneous, not very dense and it is not known to interact through any of the

fundamental forces other than gravity. In a standard Λ model (where a constant is added to the right hand side of the equation 1) it is unclustered on all scales and is constant with time (but this is not the case in other models of dark energy). Independent of its precise nature, dark energy would need a strong negative pressure in order to explain the actual acceleration in the expansion rate of the Universe. It can be demonstrated in the FRW metric, described above, that the cosmic factor \ddot{R} is positive if the equation state of the Universe is $\omega < -1/3$. According to this equation of state which causes accelerating expansion at present epochs, each cosmology model makes different predictions for the future evolution of the Universe. The current models include a cosmological constant Λ with $\omega = -1$, a phantom energy with $\omega < -1$, or a more general "quintessence" with $-1 < \omega < -1/3$.

The remaining components of the energy density are dominated by hypothetical matter (Zwicky, 1933) in a non-relativistic form of an unknown nature, called "*dark matter*", where its presence is undetectable by its emitted radiation. Evidence for dark matter comes from observations of the dynamics of galaxies and clusters, gravitational lensing and from the temperature distribution of hot gas in galaxies and clusters of galaxies. In the current scenario of structure formation, it is believed to consist of particles which interact only through the force of gravity. Observations of light elements in the universe and the theory of Big Bang nucleosynthesis dictate that it is not composed of baryons. It may be composed of particles that interact through the weak interaction; the particle candidates that have been considered include neutralinos (the lightest supersymmetric particle), exotic neutrinos, axions, jupiters and black holes of mass $< 100M_{\odot}$. These coincide with the common definition of *cold dark matter*. At early times these particles are non-relativistic, with mean velocities that are small relative to the mean expansion of the Universe (neutrinos with masses $< 30eV$ are excluded). For both the dark matter ($\Omega_{DM} \simeq 0.23$) and the baryons ($\Omega_B \simeq 0.04$), the equation of state is $\omega = 0$, and the density is diluted like $\rho \propto a^{-3} \propto (1+z)^3$. Dark matter plays an important role in structure formation because of its gravitational interaction. The gravitational Jeans instability which allows compact structures to form is not opposed by any force, such as the radiation pressure. As a result dark matter

begins to collapse into a complex network of dark matter haloes well before the ordinary matter, which is impeded by pressure forces. Without dark matter, the epoch of galaxy formation would occur substantially later in the Universe than is observed.

The expansion of the Universe, modifies the proper distance between galaxies. For this reason, the velocity of objects in the Universe have associated a “peculiar” velocity component due to the gravitational attraction of the other objects and also, what is termed as, the Hubble flow due to the recessional velocity from the observer given by the expansion factor. The expansion also causes the spectral redshift of photons, which in turn lower their frequencies and they lose energy as they propagate through the space-time. For now, the value of the Hubble constant H_0 or the measured present expansion rate of the Universe is not well parametrized in term of the dimensionless number h , where:

$$h = \frac{H_0}{100 \text{ km s}^{-1} \text{ Mpc}^{-1}}. \quad (13)$$

However, equation 2 gives the cosmological redshift when we plug $ds^2 = 0$ (null geodesic for a light ray)

$$z = \frac{a_0}{a} - 1. \quad (14)$$

The evolution of the Universe depends not only on the total density, ρ , but also on the individual contributions from the various (ith) components present, we have:

$$\Omega_i = \frac{\rho_i}{\rho_c}, \quad (15)$$

where ρ_c is defined as equation 12. Constraints on cosmological parameters have been established so far using data from different type of observations. The basic set of cosmology parameters are listed in table 1. The cosmological model defined by the current set of cosmological parameters is defined as ”standard model”. It mainly aims to provide the more accurate description of the actual and high-redshift Universe, as indicated by various observational data.

The cosmological constant and the density parameters $\Omega_{m_i} = \frac{\rho_{m_i}}{\rho_c}$ (where ρ_{m_i} is the density of the various components of mass energy: baryons, radiation, dark matter and neutrinos) plays a fundamental role in modern cosmology. From a various number

Table 1: The cosmological parameters deduced from different type of data

Parameter	Symbol	Value
Hubble constant	h	0.73 ± 0.03
Total matter density	Ω_m	$\Omega_m h^2 = 0.134 \pm 0.006$
Baryon density	Ω_b	$\Omega_b h^2 = 0.023 \pm 0.001$
Cosmological constant	Ω_Λ	0.7
Power spectrum normalisation	σ_8	0.9
Spectral index	n	1.0

of observational studies to calculate the density parameter $\Omega_m = \sum_i \Omega_{m_i}$, all of them indicate the presence of a remarkable quantity of dark matter (Sakharov and Hofer, 2003).

The present-day Universe is composed of an abundance of various structures on all scales: planets, stars, galaxies, clusters of galaxies and filamentary structures connecting clusters. However, on the large scale, the Universe appears to be homogeneous as confirmed by data from the Cosmic Microwave Background and demonstrated by the distributions and correlation functions of galaxies and clusters (2dFGRS Colless et al., 2003). Galaxies and other structures can form through gravitational collapse of overdensities set up in the early Universe, but all the processes involved in galaxy formation and evolution are not completely understood.

In general, studying issues of galaxy formation and evolution involves two complementary approaches. The first approach is to use observations of the properties of galaxies - such as the cooling of gas in haloes, the formation of stars, the feedback effects on interstellar gas released by young stars, the production of the heavy elements, the evolution of stellar populations, the effects of dust, the merging of galaxies - and attempt to work backwards to see what inferences can be drawn about how galaxies have evolved over a large fraction of cosmic history, and possibly how they were formed. However, we have limited information about very distant objects which is important in understanding the evolution of galaxies. The alternative approach to looking backwards is to consider how conditions in the early Universe are likely to have given rise to the structures we observe. This is possible because conditions in the early

Universe were remarkably uniform and predictable. The apparently complex structures of galaxy we observe in the present day Universe have evolved from these simple conditions through a range of physical processes which can be modelled. A useful tool for linking these two approaches involves simulating galaxy evolution computationally. Two different modelling techniques to calculate the evolution of dark matter and baryons have been developed:

- the direct simulations which involve the use of a variety of numerical techniques to solve the gravitational and hydrodynamical equations in the expanding universe explicitly (e.g [Katz et al., 1992](#); [Evrard et al., 1994](#); [Frenk et al., 1996, 1999](#); [Navarro et al., 1997](#); [Pearce et al., 1999](#); [Blanton et al., 2000](#));
- the semi-analytic modelling of galaxy formation which involves the use of the simple analytic models to calculate the evolution of the baryonic component (e.g. [White and Rees, 1978](#); [White and Frenk, 1991](#); [Kauffmann and White, 1993](#); [Cole et al., 1994](#)).

And the evolution of the dark matter is calculated either directly using N-body methods or using Monte-Carlo technique that follows the formation of dark matter haloes by hierarchical merging.

Using the direct simulations leads to the problem of the resolution limitation when resolving the formation and internal structure of individual galaxies in cosmological volumes. However the advantage of this technique is that the dynamics of the cooling gas are calculated in full without the need for simplifying assumptions. During the semi-analytic modelling, high resolution modelling can be carried out with less computational power, and a variation of the parameters is possible to match some of the observable galaxy properties particularly at high redshift (sizes, luminosities, M/L , circular velocities, etc.). However the main disadvantage is the need for simplifying assumptions in the calculation of gas properties. A growing body of galaxy properties has been simulated and analysed using this technique. The common semi-analytic modelling was originally proposed by [White and Rees \(1978\)](#), and further developed by [Davis et al. \(1985\)](#), [Lacey and Silk \(1991\)](#) and [White and Frenk \(1991\)](#). They showed

the overall philosophy and basic methodology of this approach. This method has been developed by two large collaborations: the MPA groups (e.g [Kauffmann and White, 1993](#); [Kauffmann et al., 1997](#); [Mo et al., 1998, 1999](#); [De Lucia et al., 2006](#)) and the Durham groups (e.g [Lacey and Cole, 1993](#); [Cole et al., 1994, 2000](#); [Heyl et al., 1995](#); [Baugh et al., 2005](#); [Benson et al., 2005](#); [Bower et al., 2006](#)). Several other groups have explored this technique to study aspects of galaxy formation and evolution (e.g [Avila-Reese et al., 1998](#); [van Kampen et al., 1999](#); [Somerville and Primack, 1999](#)).

1.3 LRGs background

Galaxies are found to occupy two distinct regions in colour-magnitude space known as the red sequence and the blue cloud ([Strateva, 2001](#); [Blanton et al., 2003](#)). There is also an underpopulated space known as the green valley between the two distributions made up with red late type galaxies. The blue cloud is made up mostly of star-forming late type galaxies, and is a broad distribution with large scatter in colour at all magnitudes. The red sequence is made up mostly of early type galaxies with little continuing star formation. From the results of the relation between mass and metallicity, early type galaxies lie along a tight colour-magnitude relation ([Bower et al., 1992](#); [Gallazzi et al., 2006](#)) in the sense that the most massive are the most metal rich and consequently redder. The amount of stellar mass contained in the red galaxies population has approximately doubled since $z = 1$ ([Faber, 2007](#)), this increasing mass is mostly caused by stellar mergers.

Luminous Red Galaxies (LRGs) are intrinsically luminous ($L > 3L^*$ we refer L^* as normal luminous galaxies) early-type galaxies ([Eisenstein, 2005](#); [Wake, 2006](#)), selected via their red colours ([Eisenstein, 2001](#)), having photometric properties consistent with an old, passively evolving stellar population ([Faber, 1973](#); [Visvanathan and Sandage, 1977](#); [Bernardi et al., 2006](#)). They are shown to have relatively homogeneous spectral properties ([Faber, 1973](#); [Eisenstein et al., 2003](#)), and identified with little recent star formation activity ([Roseboom, 2006](#)). All of these characteristics make them ideal tracers of large scale structure at intermediate redshifts ($0.3 < z < 1$).

Some characteristics of LRGs found in the literature:

- LRGs are found in and around the cores of clusters, (one can say that these objects are very similar to brightest cluster galaxies (BCG)) implying that they are good candidates to detect and study clusters at optical wavelengths. Furthermore, cluster studies provide an important tool for gauging the growth of structure and probing the density of the underlying dark matter and energy (Springel et al., 2005). They are the most massive and bright galaxies which provide us with high signal to noise ratio spectra. They have the most vigorous merger histories in the hierarchical merger model in which they increase in mass significantly from $z < 1$ (De Lucia et al., 2006). They dominate the stellar mass density of the universe (Fukugita et al., 1996; Hogg, 2002). The uniformly red and old stellar populations of LRGs have traditionally been interpreted as evidence for a formation scenario in which these galaxies form in a single intense burst of star formation at high redshift and then this star formation rate decreases to the present day (Gallazzi et al., 2005; De Lucia et al., 2006; Barber et al., 2007), indicating that the more massive a galaxy is, the earlier most of its stars were formed.
- They are strongly biased objects, having a value of $b \sim 2$ where b is the linear bias and relates in the linear regime, the underlying mass density distribution to that of the luminous tracers via $\delta_g = b\delta_m$ (Padmanabhan, 2007). Using the 2SLAQ LRG survey, Ross et al. (2008) have obtained the clustering amplitude of the LRGs. This has been exploited to constrain cosmological parameters (e.g Eisenstein, 2005; Cabré and Gaztañaga, 2009; Gaztañaga et al., 2009; Sanchez et al., 2009; Watson and Berlind, 2009) on different scales, to constrain the mass of the dark matter haloes which host these galaxies and to probe their merger history (Zehavi et al., 2005; Masjedi et al., 2006; Ross et al., 2007).
- Using the variation of the average spectrum with luminosity, environment and redshift, luminous galaxies in clusters have older stellar populations demonstrated by previous observational studies (Bower et al., 1990).

- [Barber et al. \(2007\)](#) have used the population synthesis models to estimate the mass, metallicities and star formation histories of LRGs by fitting measured spectral indices using a large library of high resolution spectra. They find that LRGs have a range of formation ages and stellar histories.
- [Conroy et al. \(2007\)](#) used N-body simulation to study the merger histories of the dark matter haloes which they assume host LRGs, they supposed that LRGs are tidally disrupted.
- [Hodge et al. \(2009\)](#) have detected and studied the properties of faint radio AGN in LRG population. They showed strong cosmic evolution between redshift range from $z = 0.2$ to $z = 0.7$ using the median-stacking technique to achieve the required sensitivity.
- The semi-analytical model of [De Lucia et al. \(2006\)](#) has also been successfully matched the luminosity, colour and morphology of local elliptical galaxies, where the more massive ones would be LRGs. [Almeida et al. \(2008\)](#) have studied properties of LRGs in hierarchical cosmology using two different models from Durham : the Bower and Baugh models, they have shown that the luminosity function and the clustering of LRGs are closely matched to the observed properties of LRGs, as well as many observables are well produced. Note that these two models have different mechanisms to suppress the formation of massive galaxies: the [Bower et al. \(2006\)](#) model uses the AGN-feedback to prevent gas from cooling in massive haloes; while the [Baugh \(2006\)](#) model involves superwinds to eject gas before it is turned into stars (See the next chapter to have more information about the two models).

1.4 Simulation characteristics

We investigate the properties of LRGs in the Λ CDM cosmology using two galaxy formation models based on the Millenium Simulation, one by De Lucia et al. (2006) (the MPA model) and the other by Bower et al. (2006) (the Durham model). Both

models have had remarkable success in producing a number of observed properties of the local and high redshift universe, including star formation rates, stellar masses and many others properties. To understand more about the formation of structure in the Universe, [Springel et al. \(2005\)](#) carried out the largest high resolution simulation of cosmic structure growth using only dark matter: the so-called Millennium Run. This simulation was performed with the code GADGET2 ([Springel et al., 2005](#)) using 2160^3 ($\sim 10^{10}$) particles of mass $8.6 \times 10^8 h^{-1} M_{\odot}$ from redshift $z = 127$ to the present in a cubic box $500h^{-1}$ on a side. The spatial resolution is $5h^{-1}kpc$ everywhere in the entire box. The initial configuration of this Λ CDM model was constructed with parameters from 2dFGRS (2 Degree Field Galaxy Redshift Survey) ([Colless, 2001](#)) and first year WMAP (Wilkinson Microwave Anisotropy Probe) ([Spergel et al., 2003](#)) data. The parameters¹ used in this work are $\Omega_m = 0.25$, $\Omega_b = 0.0045$, $h = 0.73$, $\Omega_{\Lambda} = 0.75$, $n = 1$ and $\sigma_8 = 0.9$, where the Hubble constant is $H_0 = h \times 100 km s^{-1} Mpc^{-1}$. The simulation gives the positions and velocities of all particles at each "snapshot" in time; 64 snapshots are stored from the initial redshift ($z = 127$) to the present.

Galaxy catalogues were generated using various semi-analytic models of galaxy evolution based on the simulated halo merging trees. The details of the semi-analytical models analysed here are presented originally by [De Lucia et al. \(2006\)](#) and [Bower et al. \(2006\)](#) for the MPA and Durham models respectively. Additional information on these models is given in the following papers: [Croton et al. \(2006\)](#) for the MPA model and [Cole et al. \(2000\)](#) for the Durham model. We now review and summarize the different components of the two models in the next chapter which is relevant to our work.

¹here Ω_m, Ω_b and Ω_{Λ} are the densities of all matter, baryons and dark energy respectively, in units of the critical density ($\rho_{crit} = 3H^2/8\pi G$), n is the initial power spectrum slope and σ_8 is the rms overdensity predicted today by linear theory for a sphere of radius $8h^{-1} Mpc$

Chapter 2

2 Semi-analytical models for galaxy evolution: two models



In this chapter, I give a brief outline of the two semi-analytic models, both based on the Millenium Simulation of the evolution of cold dark matter. Dark matter haloes are identified as virialized particle groups at each snapshot within the simulation using a friends-of-friends (FOF) algorithm (Davis et al., 1985). The linked particles are separated by less than 0.2 times the mean interparticle separation. Groups which contain at least 20 particles are saved, so the minimum halo mass is $1.7 \times 10^{10} h^{-1} M_{\odot}$. A version of the SUBFIND algorithm (Springel et al., 2001) is then applied in post-processing to these FOF groups to identify gravitationally bound dark matter substructures orbiting within the FOF haloes: we refer to these as subhaloes.

In the MPA model: these haloes are the actual objects that are then used to construct merging trees, which involves the determination of descendant haloes for each halo and the storage of the distinct pieces of the tree (corresponding to merger trees of haloes found at the final time) in a form that makes it convenient to "walk" these trees. Each subhalo contains one or several galaxies and these galaxies are associated with the descendant subhalo at the future output. A halo is an ensemble of all subhaloes within a FOF group. In particular the De Lucia et al. (2006) model assumes that only the galaxy located at the position of the most bound particle of the FOF halo, the central galaxy, is fed by radiative cooling from the surrounding halo.

In the Durham model: under certain conditions a FOF group may be divided into more than one independent halo. It is done if :

- i) the subhalo is outside twice the half mass radius of the parent halo, or
- ii) the subhalo kept 75% of the mass that it had at the last snapshot as part of the independent halo.

The latter condition is applicable for the subhalo whose mass was removed from its outer layers when falling into a more massive one, inasmuch as it retained its mass for the haloes which are close enough to be linked. Both conditions are designed to avoid two haloes that are temporarily joined by a tenuous particle bridge being linked together. The descendant of a subhalo is described by following the 10 most bound particles and the descendent of a halo is that halo which contains the descendant of the most massive subhalo in both models. The construction of the galaxies to populate

the merger trees of these bound structures is specified by different techniques for each model.

2.1 Gas cooling, star formation and supernova feedback

The two models employ the standard treatment of radiative gas cooling following the framework set out by [White and Frenk \(1991\)](#). It can be summarized as follows: gas cools, condenses and forms stars within a hierarchically clustered distribution of dark matter. Gas collapsing into dark matter haloes is shock heated to the virial temperature. This aspect of modelling is disputed by e.g. [Kereš et al. \(2005\)](#). As it cools and collapses, the angular momentum that it acquired prior to turn around causes it naturally to settle into a disk, which cools fastest in the centre where the density is highest. In massive systems and at late times, the cooling time is too long for the gas to form disk. Instead a quasi static hot atmosphere forms that can be extended to the virial radius of the dark halo, and thus cools and accretes onto a central cold disk. However, at early times and in lower mass systems the cooling time is very rapid so the quasi static halo cannot form and the supply of cold gas is limited purely by the rate at which gas can free-fall onto the disk; the reionization of the gas modifies the fraction of the dark matter halo with which an associated gas is initially available to cool in both models.

The two models are different from each other in terms of how they calculate the instantaneous rate of gas cooling. First of all, [Bower et al. \(2006\)](#) allow gas to accrete onto the cold disk if it lies within a cooling radius, assuming that the local cooling time is equal to the halo's age. On the other hand, [De Lucia and Blaizot \(2007\)](#), the MPA model, define the age of the halo as the time when it last doubled in mass, and then calculate a rate based on the amount of gas that has a cooling time less than the halo dynamical time. The Durham prescription typically results in higher cold gas masses than the MPA prescription by a factor of ~ 2 at $z \leq 5$ in central galaxies, rising to a factor of ~ 3.5 by $z \sim 0$. Stars are assumed to form from the cold disk gas or in a burst with [Kennicutt \(1983\)](#) and [Chabrier \(2003\)](#) initial mass functions (IMF) in the

Durham and MPA models respectively. Both models use the same stellar population model of [Bruzual and Charlot \(2003\)](#) to obtain stellar population properties.

In the Durham model, regarding quiescent star formation in discs, they adopt the assumption that the star formation timescale is depending on some power of the circular velocity of the disc and multiply this by an efficiency factor (equation 4.14 of [Cole et al., 2000](#)) which depends on the dynamical time of the galaxy. Dynamical times are shorter at high redshifts, hence the quiescent star formation timescales are very rapid. They consider that mergers can trigger starbursts and bursts will occur when discs become dynamically unstable.

The MPA model adopts the star formation prescription introduced by [Kauffmann \(1996\)](#) and recently revised by [Croton et al. \(2006\)](#). It is given by the relation:

$$\psi = \alpha(M_{cold} - M_{crit})/t_{dyn}, \quad (16)$$

where M_{cold} and $t_{dyn} = R_{disc}/V_{vir}$ are the cold gas mass and the dynamical time of the galaxy respectively, and ψ is the star formation rate. The parameter α regulates the efficiency of the conversion of gas into stars. There is a critical value of the surface density at a distance R from the galaxy centre for the cold gas above which star formation can occur:

$$\Sigma_{crit} = 1.2 \times 10^7 \left(\frac{V_{vir}}{200 \text{ km s}^{-1}} \right) \left(\frac{R}{10 \text{ kpc}} \right)^{-1} M_{\odot} \text{ kpc}^{-2}, \quad (17)$$

where V_{vir} is the halo virial velocity and from this equation M_{crit} in equation 16 is obtained. The use of the surface density threshold reproduces the observed trend of the gas fraction as a function of galaxy luminosity, due to the fact that the gas density always remains close to the critical gas surface density value ([Kauffmann, 1996](#)).

Both models regulate star formation by the injection of energy from supernovae into the cold gas reservoir. In the standard mode of supernova feedback, supernova injects gas, metals and energy into the surrounding medium, the cold disk gas is heated and possibly ejected from the galactic disk by changing the composition of the surrounding hot gas and modifying its cooling time. Star formation in the disk affects its development significantly.

2.2 Mergers and disk instability

Figure 1 illustrates a summary of the hierarchical galaxy formation model without considering the subhalo concept. Galaxy mergers and disk instability are responsible for disturbing the stellar disk. Galaxy mergers are a result from the mergers of the haloes that host them, and they particularly shape the evolution of galaxies, by affecting their morphology and their star formation histories. As mentioned earlier, a halo that falls into a more massive system may survive (for sometime thereafter) as a gravitationally bound subhalo. Thus a less massive (satellite) galaxy can be followed explicitly until tidal effects disrupt its subhalo sufficiently for it to drop below 20 particles (the resolution limit). In the MPA model, the galaxy is associated with the most bound particle of the subhalo just before it became unresolved. The satellite's orbit is assumed to decay through dynamical friction against the halo material until it merges with the more massive (central or primary) galaxy. Merger timescales are determined differently in the Durham model, with the satellite's orbit chosen at random from the cosmological distribution derived by [Benson et al. \(2005\)](#), as soon as the halo merger has taken place and a dynamical friction timescale calculated consequently, i.e. a time, $t_{friction}$, when the satellite galaxy is merged with the central galaxy after its own subhalo was last identified. It is obtained using the dynamical friction formula of [Binney and Tremaine \(1987\)](#):

$$t_{friction} = 1.17 \frac{V_{vir} r_{sat}^2}{GM_{sat} \ln \Lambda}, \quad (18)$$

which is valid for a satellite galaxy of mass M_{sat} orbiting in an isothermal halo of circular velocity V_{vir} at radius r_{sat} . M_{sat} and r_{sat} are the values measured for the satellite galaxy at the last time its subhalo could be identified. The Coulomb logarithm is defined as:

$$\ln \Lambda = \ln \left(1 + \frac{M_{vir}}{M_{sat}} \right), \quad (19)$$

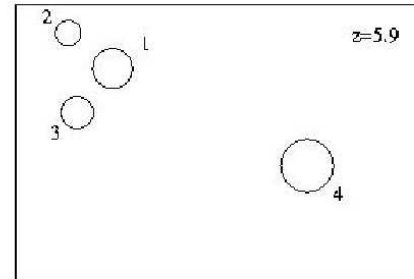
where M_{vir} is the virial mass of the central galaxy.

In the Durham model, [Lacey and Cole \(1993\)](#) estimated the merger time based on the standard Chandrasekhar formula for the dynamical friction, written as:

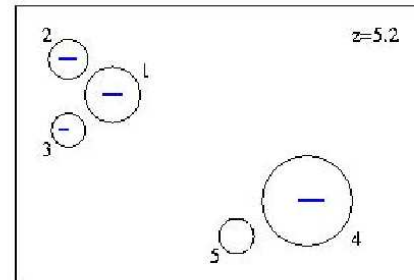
$$t_{merger} = f_{df} \theta_{orbit} t_{dyn} \frac{0.3722}{19} \frac{M_{cen}}{M_{sat}}. \quad (20)$$

Modelling Hierarchical Galaxy Formation: An Illustration

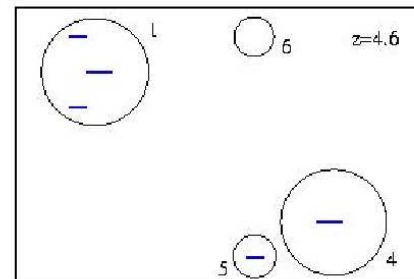
1. Four dark matter halos identified in simulation



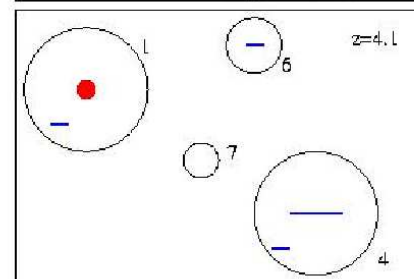
2. Gas cools into disks in halos 1–4 and forms stars
Halo 5 collapses



3. Halos 2 and 3 merge with Halo 1 .
Galaxy 1 is central, galaxies 2 and 3 are satellites
No cooling onto 2 & 3, only onto 1
Halo 4 grows, more gas cools, more stars form
In Halo 5, gas cools and forms stars
Halo 6 collapses



4. Galaxy 2 merges with galaxy 1 on dynamical friction timescale. They have similar size so spheroid formed.
Galaxy 3 still a satellite.
Halos 4 and 5 merge, galaxy 5 becomes satellite
Gas cools in halo 6 and stars form
Halo 7 collapses



5. More gas cools into disk around galaxy 1
Galaxy 3 still a satellite
Galaxy 5 merges with galaxy 4 but much smaller
so no spheroid formed
Halo 6 grows, more gas cools, more stars form
Gas cools into halo 7 and forms stars

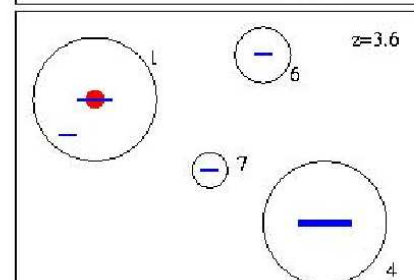


Figure 1: Hierarchical galaxy formation simplified by neglecting the "subhalo" concept.

Here M_{sat} is the mass of the satellite galaxy including the mass of the dark halo in which it formed (Navarro, 1995); M_H is the mass of the halo in which the satellite

orbits; θ_{orbit} is the orbital parameters defined as:

$$\theta_{orbit} = [J/J_c(E)]^{0.78} [r_c(E)/r_{vir}]^2, \quad (21)$$

where E and J are the initial energy and angular momentum of the satellite's orbit, and $r_c(E)$ and $J_c(E)$ are the radius and angular momentum of a circular orbit with the same energy as that of the satellite; and the Coulomb algorithm defined as:

$$\ln\Lambda = \ln\left(\frac{M_H}{M_{sat}}\right). \quad (22)$$

here the dynamical time of the halo is :

$$t_{dyn} = \pi r_{vir}/V_H, \quad (23)$$

and f_{df} is the dimensionless parameter greater than unity if the infalling satellite's halo is efficiently stripped off early on.

The result of each merger depends on both the relative mass of the merging satellite galaxies, M_{sat} , and the gas content of the central galaxies, M_{cen} , (Kauffmann and White, 1993; Baugh et al., 1996). The merger is major if $M_{sat}/M_{cen} \geq 0.3$ and is destroying the disk of both galaxies to form a spheroid which contains all stars from its progenitor galaxies. Any gas present in the disks of the merging galaxies forms stars in a burst, which are also forming a part of a new spheroid, with some amount of gas being returned to the hot halo through supernovae feedback. However, the merger is classed minor if $M_{sat}/M_{cen} < 0.3$. The structure (angular momentum) of the central galaxy is intact but the stars of the accreted satellite are added to the bulge of the primary and its gas to the main gas disk. The merger may establish a burst if $M_{sat}/M_{cen} \geq 0.1$ and the central galaxy has sufficient gas in its disk $M_{gas}/M_{disk} > 0.1$. The fraction of the available gas that is turned into stars is dictated by star formation and feedback rules, applied over the timescale of the burst.

In the MPA model, all mergers produce starbursts. This process has been discussed by Croton et al. (2006). In general all mechanisms are similar to the Durham model. Major mergers are defined in the same way and end up in the formation of a spheroid, during minor merger stars are added to the primary's bulge and gas to its disk. In

this model the mass fraction of the combined cold gas from the two galaxies which is turned into stars after merger, is defined as:

$$e_{burst} = \beta_{burst}(M_{sat}/M_{cen})^{\alpha_{burst}}, \quad (24)$$

where β_{burst} and α_{burst} are fitted parameters.

The disk instability has been discussed in detail by [Mo and Mao \(2000\)](#) & [Cole et al. \(2000\)](#). While a massive disk has a strong self-gravity, it becomes unstable to small perturbations by minor satellites or dark matter substructures. They concentrate on the complete merging history of the bulge component and the disk, and use for the stability criterion, the quantity:

$$\epsilon_m = \frac{V_{max}}{(GM_{disk}/r_{disk})^{1/2}}. \quad (25)$$

Here V_{max} is the circular velocity at the disk half radius r_{disk} in the Durham model, and approximately the halo virial velocity in the MPA model, M_{disk} is the disk mass. If $\epsilon_m \geq 1.1$ at any time-step, the disk is considered to be unstable. Then the whole mass of the disk is transferred to the galaxy bulge with any gas present assumed to undergo a starburst. The size is imposed by the rotational energy of the disk just prior to collapse. As with a major merger, a starburst is induced such that the resulting spheroid contains the original disk's stars plus those formed in the burst. This more catastrophic termination is assumed to result from orbital resonances and stellar scattering in a barred system causing it to collapse entirely.

Whereas in the MPA model, there is effectively a partial collapse, intended to model the formation of the bar. Mass is transferred from the disk into the spheroid until the stability of the system defined by the equation above is re-established. This process plays an important role in the growth of black holes as a fraction of the gas goes into feeding the central BH, (see the section below).

2.3 Black holes and AGN feedback

In both models, they have added the prescriptions of supermassive black hole (BH) growth and feedback from active galactic nuclei (AGN) inspired by the growing evidence that there is a link between properties of a galaxy's bulge and the mass of its central BH (e.g. [Ferrarese and Merritt, 2000](#)).

The full details of the prescription used in the Durham model for AGN feedback and BH growth are described by [Malbon et al. \(2007\)](#), and it is based on the model of [Kauffmann et al. \(2000\)](#). A BH is assumed to grow through four main channels:

- i) *Major merger-driven accretion* : tidal forces act to drive disk gas into central regions, fuelling the BH. A constant fraction of the accreted gas, f_{BH} (tuned to match the amplitude of the $M_{BH} - M_{Bulge}$ relation) is added to the BH, from that stars formed during starburst induced by a merger.
- ii) *Instability-driven accretion*: a fraction f_{BH} of the gas in the collapsing disk is added to the BH.
- iii) *BH-BH mergers*: during the merging of two galaxies, their BH are assumed to merge. Mass loss due to the radiation of gravitational waves is neglected and the mass of the new BH is the sum of the progenitors plus any gas accreted.
- vi) *Accretion from cooling flows*: during quasi-hydrostatic cooling in massive haloes, BHs can accrete mass from the cooling flow. This latter channel is associated with the implementation of AGN feedback in this model. The AGN feedback is assumed to be effective in haloes where a quasi-static hot haloes has formed. The energy input through the accretion is considered to associate efficiently with the hot halo gas.

Instead of assuming the phenomenological dependence of the strength of the feedback on the gas temperature or BH mass, [Bower et al. \(2006\)](#) consider that the flow will adjust itself so as to balance heating and cooling whenever the Eddington luminosity of the BH is sufficiently large. If the energy generated from the BH (the jet power) exceeds the rate limit at which the gas can radiate away energy then no further gas is allowed to cool. Hence, as soon as a large cooling flow builds up, feedback becomes sufficient to cut it off. This is important in producing the observed K and B-band

luminosity functions out to $z = 5$. The cooling of gas is suppressed in massive haloes due to the heating of the halo gas by the energy released by the accretion of matter onto a central supermassive BH.

On the other hand, MPA's prescription of AGN feedback considers that gas inflows occur in all mergers with the accreted fraction of the total gas dependent on the satellite-central mass ratio. This prescription is detailed in [Croton et al. \(2006\)](#). They assume three modes of AGN growth within galaxies:

- i) merging between black holes modelled in a similar way as in the Durham model,
- ii) the quasar mode accretion which dominates the growth of the BH at high redshifts since it is modelled as a direct sum of the progenitor BH masses without considering the gravitational waves losses. They assume that the gas mass accreted \dot{m}_{BH} during the merger is proportional to the total cold mass present m_{cold} , but with an efficiency which is lower for smaller mass systems and for unequal mergers:

$$\dot{m}_{BH} = \frac{f'_{BH} m_{cold}}{1 + (280 \text{ km s}^{-1} / V_{vir})^2}, \quad (26)$$

where $f'_{BH} = f_{BH}(M_{sat}/M_{cen})$. The contribution of minor mergers to the growth of the BH and the growth of the bulge is small, however the accretion driven by major mergers is the dominant mode of BH growth (the quasar mode). This mode of accretion is closely associated with starbursts.

- iii) the radio mode accretion which becomes important at low redshifts where it quenches the cooling flows by injecting sufficient energy into the surrounding medium, but is an insignificant contributor to the overall BH mass density. The outflows generated by this accretion have a major impact on the final galaxy properties particularly in higher mass haloes (galaxy luminosity function, colours, stellar masses and the clustering of galaxies that populate the bright end of the galaxy luminosity function). The phenomenology to describe the accretion from quasi-hydrostatic cooling flows is summarized by a simple relation between the mass accretion rate \dot{m}_{BH} , the BH mass m_{BH} , the hot gas fraction f_{hot} and the virial velocity of the halo V_{vir} .

$$\dot{m}_{BH} = \kappa_{AGN} m_{BH} f_{hot} V_{vir}, \quad (27)$$

where κ_{AGN} is the free parameter to control the efficiency of the accretion. The luminosity of the BH is described as :

$$L_{BH} = \eta \dot{m}_{BH} c^2, \quad (28)$$

where $\eta \simeq 0.1$ is the standard efficiency of mass energy conversion expected near the event horizon, and c is the speed of the light. From this energy generated, a modified cooling rate is calculated and it is maintained as the amount of mass accreted increases.



Chapter 3

3 Identifying LRGs



3.1 The Millenium Run database

All the data analysed in this thesis comes from the online Millenium Run database², developed by the German Astrophysical Virtual Observatory (GAVO) team, which can be accessed using the structured query language (SQL) (Lemson and Virgo Consortium, 2006). Detailed assembly histories of all galaxies, all haloes and all subhaloes resolved by the simulation from two independent models of galaxy formation (the Durham and MPA models) are stored. Different properties are associated with each halo and galaxy such as position in the box, velocity, redshift, number of subhaloes etc. In addition, galaxies carry many directly and indirectly observable properties including the rest frame and observer frame magnitudes in various passbands, star formation rates, metallicity, stellar mass, halo mass etc. The database has been constructed to make the retrieval of the merger tree structure, which describes the assembly history of all objects, as efficient as possible (Lemson and Springel, 2006). This has been achieved by assigning unique IDs in a depth-first order, such that the progenitors of a given object have IDs lying between the object itself and an index, called lastprogenitorid. Progenitors can thus be easily located. Additional identification indices for each object's immediate descendant and largest progenitor are provided. An additional index in the Durham tables identifies every galaxy's main branch.

3.2 LRGs selection criteria

In this section, I present tests of the two model predictions for the abundance and properties of LRGs. We use two independent selections of LRGs, the Sloan Digital Sky Survey (SDSS) (York, 2000) LRGs target selection and a cut based on the rest frame luminosities. Originally, we extracted LRGs using the selection criteria from the SDSS described by Eisenstein (2001), based on their colours and apparent magnitudes to yield a sample of intrinsically luminous and red galaxies. They extend fainter and farther than the main flux limited portion of the SDSS galaxy spectroscopic sample. The red colour selection isolates galaxies with a strong 4000 Å break and a passively

²Hosted at <http://www.mpa-garching.mpg.de/millennium> which require registration for full access

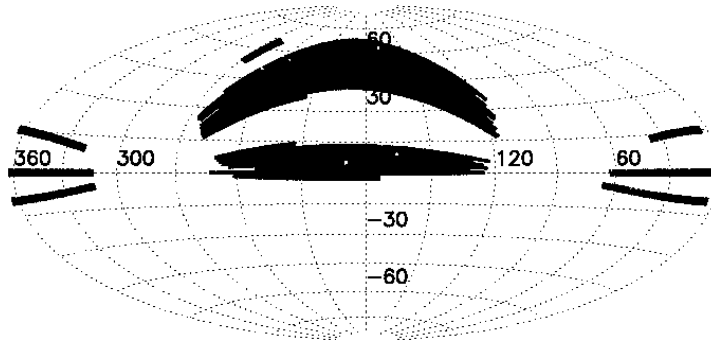


Figure 2: The sky coverage of the SDSS imaging survey. Credit from the Sloan Digital Sky Survey website (www.sdss.org)

evolving stellar population. It is the redshifting of this break through different filters enables LRG discovery via photometry over a large redshift range. The basic goal of LRG surveys is to select intrinsically bright galaxies which have colours consistent with those expected for a passively evolving stellar population (Eisenstein, 2001).

The SDSS is a photometric and spectroscopic survey using a 2.5 m telescope (Gunn, 2006), mapping Π steradians of the sky (Figure 2). It has imaged more than 180 million objects using five filters u, g, r, i, z (Fukugita et al., 1996) and has taken spectra of 40 - 60% of them, including 560 000 galaxies. The images are processed and calibrated, allowing selection of galaxies, quasars and stars for spectroscopy with twin fiber fed double spectrographs. The SDSS LRG sample covers approximately 19% of the sky. Figure 3 shows the distribution of the SDSS LRG and 2SLAQ LRG catalogues.

A summary of the colour and magnitude ranges which define the LRG samples are described below. In the case of the observational samples, Petrosian magnitudes were used for apparent magnitude selection and SDSS model magnitudes were used for colour selection. The SDSS target selection is based on two combinations of the g-r and r-i colours:

$$c_{\perp} = (r - i) - (g - r)/4 - 0.18 \quad (29)$$

$$c_{\parallel} = 0.7(g - r) + 1.2(r - i) - 0.18 \quad (30)$$

Cut I for $z < 0.4$:

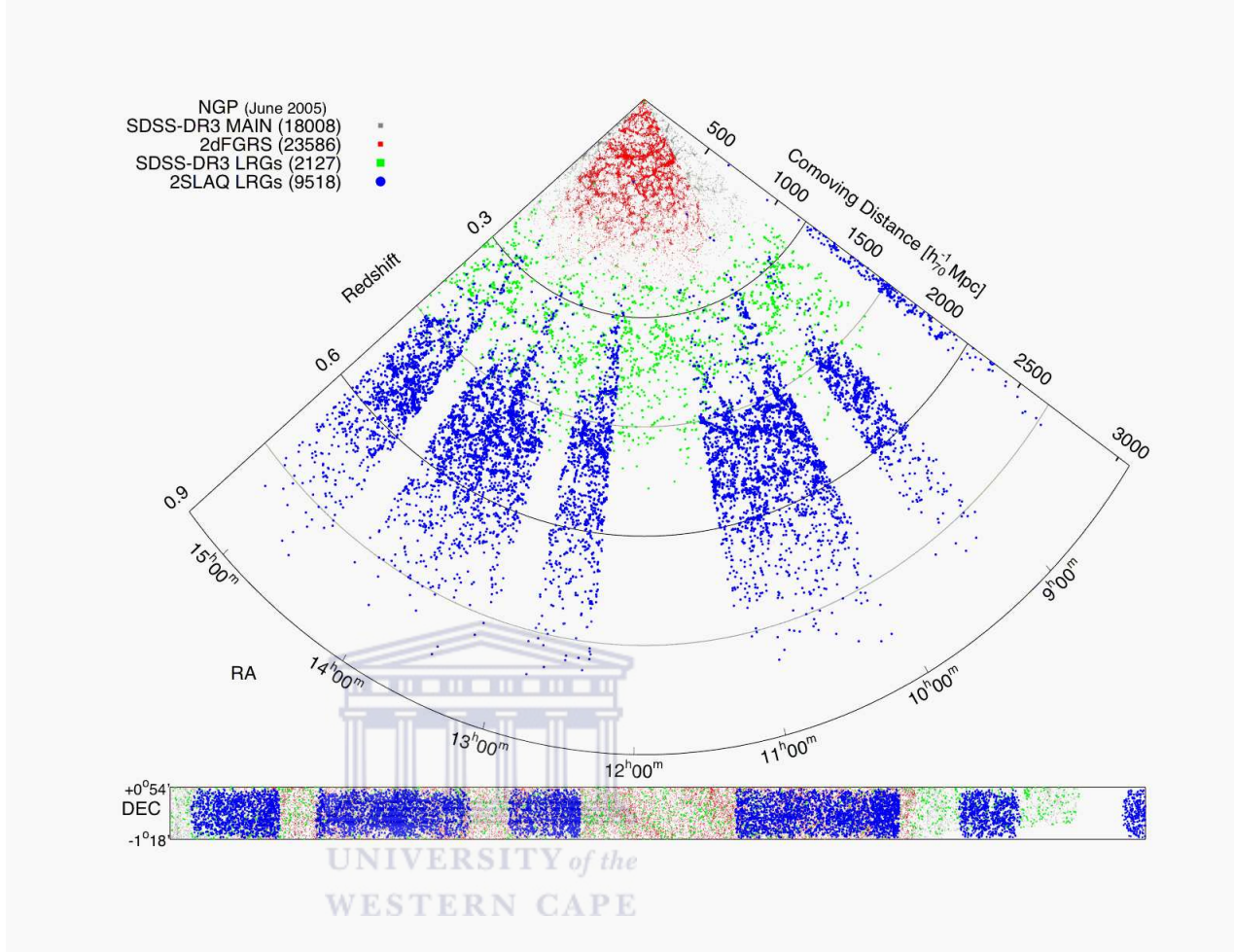


Figure 3: The distribution of the SDSS LRG and 2SLAQ catalogues. **Black points**: main galaxies from the SDSS-data release 3 (SDSS-DR3); **red points**: main galaxies from the 2SLAQ; **green points**: LRGs from the SDSS-DR3; **blue points**: LRGs from the 2SLAQ. Credit from the 2SLAQ website (www.2slaq.info)

$$r_{petro} < 1.92 \quad (31)$$

$$r_{petro} < 13.1 + c_{\parallel}/0.3 \quad (32)$$

$$|c_{\perp}| < 0.2 \quad (33)$$

Cut II for $z > 0.4$:

$$r_{petro} < 19.5 \quad (34)$$

$$c_{\perp} > 0.45 - (g - r)/6 \quad (35)$$

$$g - r > 1.30 + 0.25(r - i) \quad (36)$$

The colour equations 29, 30 and the conditions applied to them 33, 35 are designed to locate LRGs. Particularly, equations 35 and 33 are applied to identify the galaxies in high-redshift region and at the low-redshift locus. Equations 31, 32 and 34 are luminosity thresholds. Equation 36 isolates intrinsically red galaxies and separates the selected region from the bulk of the late-type stellar locus. (See Eisenstein, 2001, for more details). In the case of galaxies predicted, we use the total magnitude (absolute magnitude).

Our target redshift is close to the transition from Cut I to Cut II. The colour of these objects evolves with redshift according to the observational basis and because of the evolution of the objects with time. Around $z = 0.4$, the 4000 Å break moves to the r-band and a different colour selection is set up to select LRGs. To obtain high resolution spectra for the future experiment, we also investigate a cut in absolute magnitude restframe luminosities to cover the transition problem at $z = 0.4$. Note that this approach would be feasible in a real age-dating experiment given the availability of low-resolution spectra of large numbers of LRGs. For the two models explored in this study, at each redshift step, we select objects brighter than -23 mag in the V-band restframe, and have a colour greater than 0.81 in B-V colour. Before establishing this cut limit, we studied the effect of varying the colour and brightness cuts against the mass weighted ages of galaxies. We optimized the cut to obtain galaxies which have the narrowest distribution in mass weighted ages and SFHs: i.e galaxies that have more of their stars formed at earlier times. Figure 4 demonstrates the effect of this variation in colour and brightness at $z = 0.51$. We see that the SFR of LRGs is not sensitive to the changes of the rest-frame colour cuts in the de Lucia et al. model.

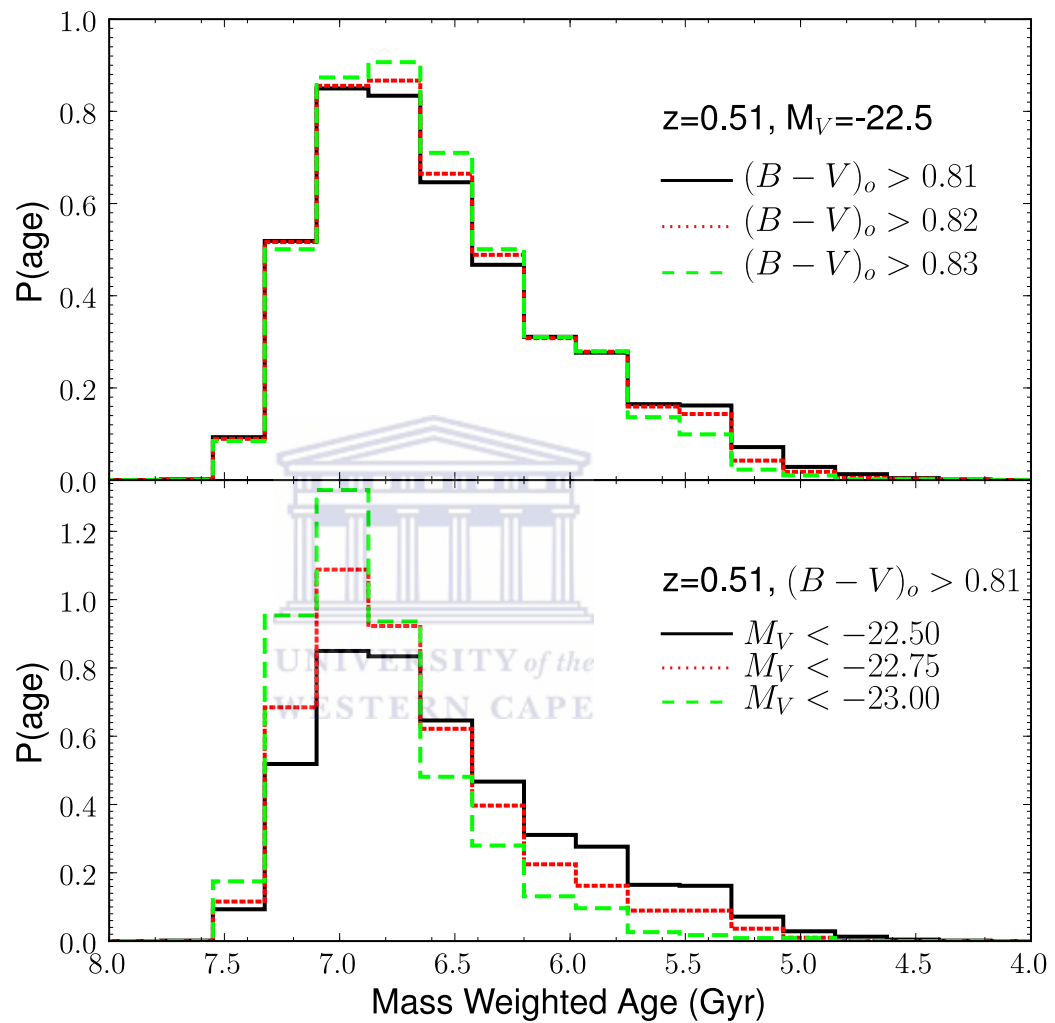


Figure 4: The effect of varying the brightness cut (top panel) and the colour cut (bottom panel) on the mass-weighted age histogram for galaxies at $z = 0.51$. Sample extracted from the de Lucia et al. model.

Chapter 4

4 Properties of LRGs



In this chapter, I present a range of predictions for the properties of galaxies which satisfy the LRG selection criteria described in the previous chapter using the de Lucia et al. model which is one of the MPA models and the Bower et al. model which is one of the Durham models. We try to compare with observational results from the SDSS samples or with observational properties of LRGs. Luminous red galaxies are a subset of the overall early-type galaxies with extreme luminosities and colours, hence it is essential to match their selection criteria as closely as possible to the observational criteria in order to consider the test of the model predictions. We begin with the abundance of LRGs predicted by the two models before moving on to examine the different properties of these galaxies in the Λ CDM cosmology. We investigate if the LRG ages depend on the environment. We plan to measure the expansion rate of the Universe at $z \sim 0.5$, thus concentrate our study around this redshift.

4.1 The abundance of LRGs

It is important to notice that LRGs represent only a small fraction of the galaxy population as a whole. Reproducing the abundance of such rare galaxies represents a strong challenge for any theoretical model. The two models predict different numbers of LRGs using both the SDSS and absolute magnitude cuts. However, they both produce small numbers of objects extracted using SDSS cuts and the number of objects is decreasing when we go to the higher redshift as quoted in table 2. When using the SDSS criteria in the de Lucia et al. model at $z=0.46$, we appear to be missing objects. This redshift is close to the redshift where the SDSS Cut I must be replaced with the Cut II, and possibly explains the missing number of objects at this redshift. Using the two models, different types of galaxies are selected near the redshift threshold. In the Bower et al. model, we obtain a small number of LRGs at each redshift even when using our absolute magnitude cuts. Since we need a number of LRG-like galaxies to complete the study, we reduced the limit of our absolute magnitude cuts in this model by 0.05 mag; this means that our final cuts are $M_V < -22.75$ and $B - V > 0.81$. Our final samples are presented in the table 2.

Table 2: Number of objects using the two different selection criteria extracted from the two catalogues.

z	De Lucia model		Bower model	
	SDSS cuts	Absolute mag cuts	SDSS cuts	Absolute mag cuts
0.32	2139	1705	3265	207
0.46	179	1491	626	138
0.51	197	1448	75	131
0.56	2	1337	11	123

The integrated number densities of LRGs in the two models are listed in table 3. Note that the box volume of the full MS is about $3.21 \times 10^8 \text{ Mpc}^3$. We compare the predictions of the two models for the abundance of LRGs with observational estimates. We used the absolute magnitude cuts to extract a sample of galaxies from the SDSS catalogue³ data release 7 (DR7) (Abazajian, 2009) at redshift ranges: $0.28 < z < 0.36$ for the case of $z = 0.32$ within $1.11 \times 10^9 \text{ Mpc}^3$; $0.41 < z < 0.48$ for the case of $z = 0.46$ within $1.65 \times 10^9 \text{ Mpc}^3$; $0.48 < z < 0.54$ for the case of $z = 0.51$ within $1.75 \times 10^9 \text{ Mpc}^3$; $0.54 < z < 0.6$ for the case of $z = 0.56$ within $2.05 \times 10^9 \text{ Mpc}^3$, exactly satisfying the following criteria :

$$R < -23.25 \quad (37)$$

and

$$G - R > 0.68 \quad (38)$$

after applying derived calculation. The space densities of the observed SDSS LRGs samples at each redshift bin are listed in table 3. Both models therefore underpredict the abundance of LRGs by a large factor. At $z = 0.51$ the absolute magnitude cut in the de Lucia et al. model predicts only $\sim 30\%$ more LRGs than the observed value, while the Bower et al. model is closer at $z = 0.56$. This result suggests that neither

³The SDSS web site: www.sdss.org

model is able to accurately predict the evolution of the luminosity function of very red galaxies over large look-back times. We do, however, believe that in the de Lucia et al. model at $z = 0.51$ we do select galaxies which are comparable with the observed LRG sample. The abundance of LRGs appears quite sensitive to the way in which feedback processes are implemented in massive haloes, especially the prescriptions for BH growth and AGN feedback or to the other differences in the two models.

Table 3: The space density of LRGs predicted by the two models using the SDSS and absolute magnitude cuts compared with the space density of observed LRG-like objects extracted from SDSS database using our absolute magnitude cuts.

z	SDSS cuts	De Lucia et al. model ($10^{-6} Mpc^{-3}$)		Bower et al. model ($10^{-6} Mpc^{-3}$)		Observed SDSS ($10^{-6} Mpc^{-3}$)
		Absolute mag cuts	SDSS cuts	Absolute mag cuts	SDSS cuts	
0.32	6.66	5.31	10.17	0.64		21.28
0.46	0.55	4.64	1.95	0.42		10.76
0.51	0.61	4.51	0.23	0.40		3.11
0.56	0.006	4.16	0.03	0.38		0.04

4.2 Star formation history of LRGs

The two models trace the full star formation of galaxies. This and especially the merger history of LRGs help us to build up a picture of how the stellar mass of LRGs was assembled and how this changes with redshift. Basically, in hierarchical models a galaxy can acquire stellar mass in two ways: through the formation of new stars and through the accretion of pre-existing stars in galaxy mergers (Baugh et al., 1996; Kauffmann, 1996).

Figure 5 shows the average star formation histories (SFH) of typical LRGs predicted in the two models using the different selection criteria described in a previous chapter. The SFHs shown in the plots of the two cuts represent the averages computed from all LRGs in the simulation box, and are the sum of the star formation rate (SFR) of all

progenitor galaxies at each redshift. In the case of the de Lucia et al. model, the star formation rate of each galaxy in the full box is provided in the database, so it is easy for us to sum up all the star formation rates for all progenitor galaxies. However, in the Bower et al. model, we have tried another method to compute the star formation rate of each simulated LRG by using its total luminosity in the $H\alpha$ emission line ($L(H\alpha)$). Since there is an empirical method for measuring star formation rates in galaxies which is the relation between the star formation rate and the total luminosity in $H\alpha$ given by the relation of [Kennicutt et al. \(1999\)](#) :

$$SFR(M_{\odot}yr^{-1}) = 7.9 \times 10^{-42}L(H\alpha)(ergs\ s^{-1}). \quad (39)$$

We are thus able to convert the $H\alpha$ luminosity given in the database to a star formation rate of LRGs in this model. This method has been explored by many researchers (e.g [Kennicutt et al., 1999](#); [Yan et al., 1999](#)) using the integrated $H\alpha$ luminosity density of the observed galaxies.

4.2.1 Results in the de Lucia et al. model

LRGs are massive galaxies with very little ongoing star formation; they thus constitute the tip of the red sequence. Modelling of their spectral energy distributions has led to the conclusion that these galaxies formed the bulk of their stars mostly at early times and evolve passively for $z \sim 1$ onwards (e.g [Trager et al., 2000](#); [Thomas et al., 2005](#); [Jimenez and Haiman, 2006](#)). Using the two different cuts, we find the LRGs in the de Lucia et al. model are consistent with these observations: at each redshift, the SFH peaks at $z \sim 5$ (z_p) with only a small amount of ongoing SFR, and the redshift of last major star formation epoch (z_e) is at $z > 1$ (where z_e is defined as the redshift where the SFR falls below $10M_{\odot}yr^{-1}$). In addition LRGs are formed earlier in this model, and they also seem massive especially for galaxies ending up in overdense regions. When looking at the star formation rate average, the LRG SFR can reach $500M_{\odot}yr^{-1}$ which is not the case when we looked at the SFR of the randomly selected galaxies at $z = 0.32$ as in figure 6.

Figure 6 shows that individual star formation histories display a much more bursty

Table 4: Formation properties of LRGs

Model	Cut	z	z_f	z_p	z_e	Age_{mw}	f_{sfr}^a	$f_{3\sigma}$
De Lucia et al.	sdss	0.32	11.86 ± 1.30	4.95 ± 1.26	1.46 ± 0.49	8.32 ± 0.28	0.32	0.13
	sdss	0.46	11.94 ± 1.23	5.06 ± 1.46	1.44 ± 0.44	7.05 ± 0.35	0.03	0.19
	sdss	0.51	12.17 ± 1.16	5.05 ± 1.18	1.49 ± 0.47	6.87 ± 0.22	0.29	0.17
	abs cut	0.32	11.94 ± 1.23	4.91 ± 1.14	1.48 ± 0.47	8.29 ± 0.27	0.14	0.15
	abs cut	0.46	11.92 ± 1.23	4.96 ± 1.18	1.54 ± 0.48	7.20 ± 0.29	0.14	0.15
	abs cut	0.51	11.89 ± 1.25	5.00 ± 1.21	1.58 ± 0.47	6.83 ± 0.31	0.14	0.15
	abs cut	0.56	11.90 ± 1.24	5.05 ± 1.26	1.62 ± 0.47	6.46 ± 0.38	0.14	0.13
	sdss	0.32	7.76 ± 1.25	2.08 ± 1.12	1.26 ± 0.66	5.44 ± 0.97	0.24	0.08
Bower et al.	sdss	0.46	9.43 ± 1.73	3.25 ± 1.84	1.53 ± 0.49	5.59 ± 1.46	0.27	0.14
	sdss	0.51	9.86 ± 1.71	3.53 ± 1.71	1.50 ± 0.40	5.51 ± 1.39	0.27	0.07
	sdss	0.56	8.71 ± 1.37	2.11 ± 1.50	1.59 ± 0.45	4.24 ± 1.22	0.63	0.10
	abs cut	0.32	10.19 ± 1.36	3.88 ± 1.70	1.53 ± 0.40	7.40 ± 1.28	0.02	0.11
	abs cut	0.46	9.82 ± 1.52	3.46 ± 1.71	1.49 ± 0.48	6.12 ± 1.43	0.04	0.10
	abs cut	0.51	9.43 ± 1.63	3.08 ± 1.67	1.53 ± 0.55	5.50 ± 1.83	0.17	0.18
	abs cut	0.56	9.35 ± 1.45	3.03 ± 1.54	1.59 ± 0.51	5.17 ± 1.04	0.25	0.16

Notes:

z_f : the formation redshift.

z_p : the redshift of peak star formation.

z_e : the redshift of last major star formation epoch.

Age_{mw} : the average of mass-weighted age.

f_{sfr}^a : the fraction of galaxies with $SFR > 5M_{\odot}yr^{-1}$ within 1 Gyr of the redshift.

$f_{3\sigma}$: the fraction of galaxies with SFR greater than 3σ away from the average SFR.

behaviour than those in figure 5 of LRGs. This behaviour reflects the assumption in the de Lucia et al. model that bulge formation takes place during a merger-induced burst, which naturally gives the SFH of individual systems a bursty nature quite different from the smooth history as seen in the average SFH. Our result of LRG SFHs predicted by the simulation in the de Lucia et al. model tends to be similar to the typical models considered in the literature (e.g Barber et al., 2007). The SFH here has a gaussian-exponential shape consistent with the idea that our LRG selections isolate a subset of galaxies with more passive star formation histories. Some of the peak values of the individual LRG SFHs are low which indicate that for the bulk of LRGs in the model, ongoing star formation is not an important channel for increasing the stellar mass of LRGs given the large stellar masses predicted for these galaxies (Almeida et al., 2008). The dataset include a few LRGs which have ongoing star formation rates at lower

redshifts; compared to the observational studies using the 2SLAQ LRG survey, this is not a surprise because some of the SDSS LRGs are found to have some recent star formation activity (Roseboom, 2006). Using the absolute magnitude cuts, almost 14% of LRGs selected in the de Lucia et al. model have had a burst of star formation greater than $5M_{\odot}yr^{-1}$ in the previous gigayear and up to 15% are more than 3σ away from the average star formation history. Table 4 summarises the average formation parameters.

Using the SDSS cuts, there is a significant dispersion in all the average formation parameters in table 4 for the population extracted in the same model: almost 30% of LRGs have had a burst of star formation greater than $5M_{\odot}yr^{-1}$ in the previous gigayear and up to $\sim 20\%$ are greater than 3σ away from the average star formation history. In passing at $z = 0.46$, as mentioned earlier, in the same model this redshift is close to the changing redshift bin within which the SDSS colour cut is defined, which affects the number of galaxies that are defined as LRGs. In addition by using this cut, when we track galaxies through various snapshots looking at their progenitors, we find that some of the galaxies drop out of the sample due to the selection criteria for LRGs at this specific redshift. The underlying sample of LRGs is thus not very homogeneous. However the determination of $H(z)$ requires the use of the oldest galaxies by measuring the age of a large number of galaxies which is not the case here. To get a more homogeneous sample we consider the absolute magnitude cuts more valuable than the SDSS cuts. It is clear looking at the top panel of figure 5 in the de Lucia et al. model that these galaxies have a more homogenous SFH compared to the bottom panel.

4.2.2 Results in the Bower et al. model

In comparing the results from the de Lucia et al. model with those of Bower et al. model, we notice significant differences. As in figure 5, LRGs have SFRs as high as $700M_{\odot}yr^{-1}$ except at $z = 0.32$ using the SDSS cuts the SFH average is flat; this is probably due to the smaller number of objects we have picked. All average SFRs of LRGs in the Bower et al. model are formed and peaked at progressively lower redshifts

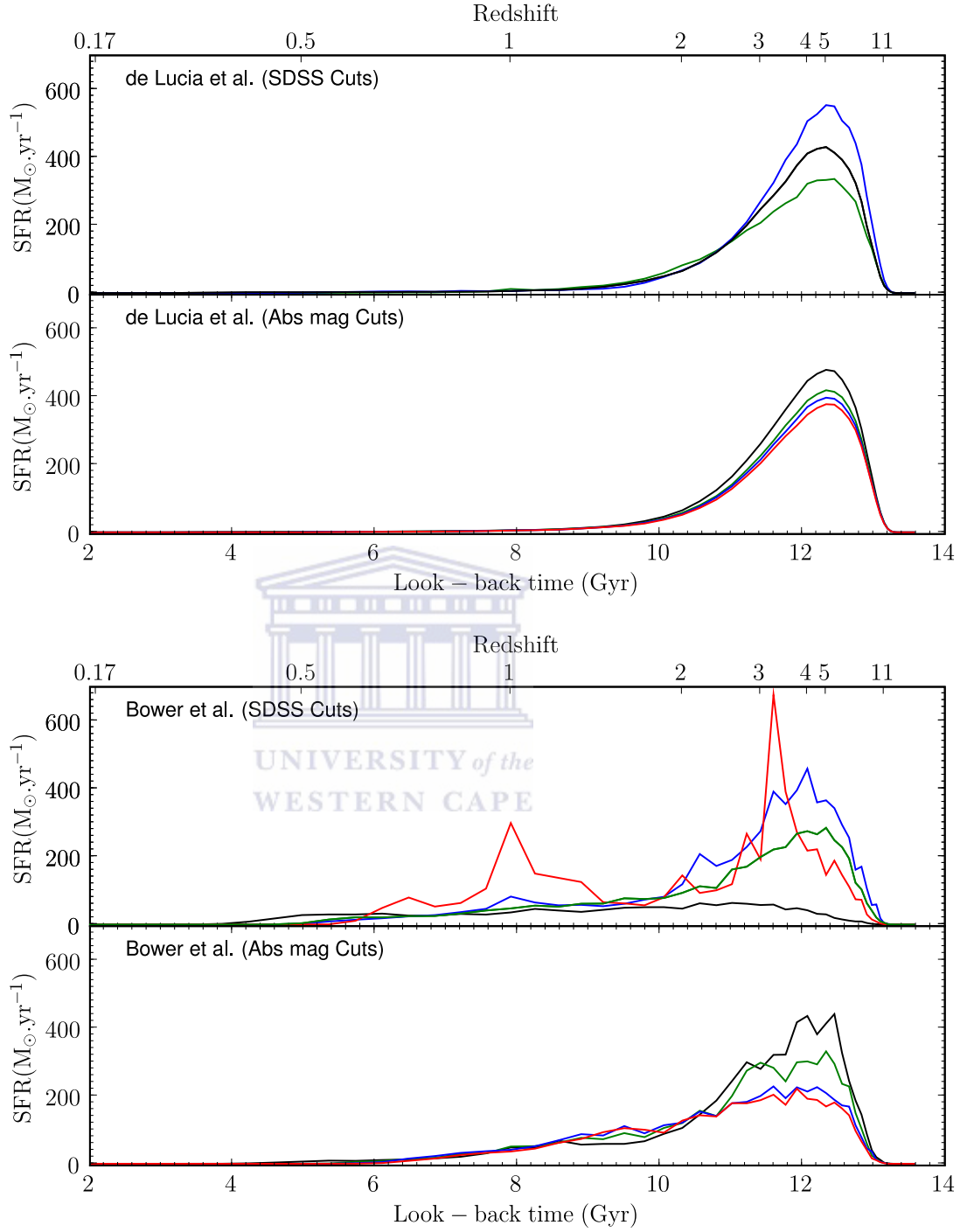


Figure 5: The average SFR using SDSS and absolute magnitude cuts in **upper panel**: the de Lucia et al. model; and **bottom panel**: the Bower et al. model. Black lines represent the average SFR at $z = 0.32$; green at $z = 0.46$; blue at $z = 0.51$ and red at $z = 0.56$.

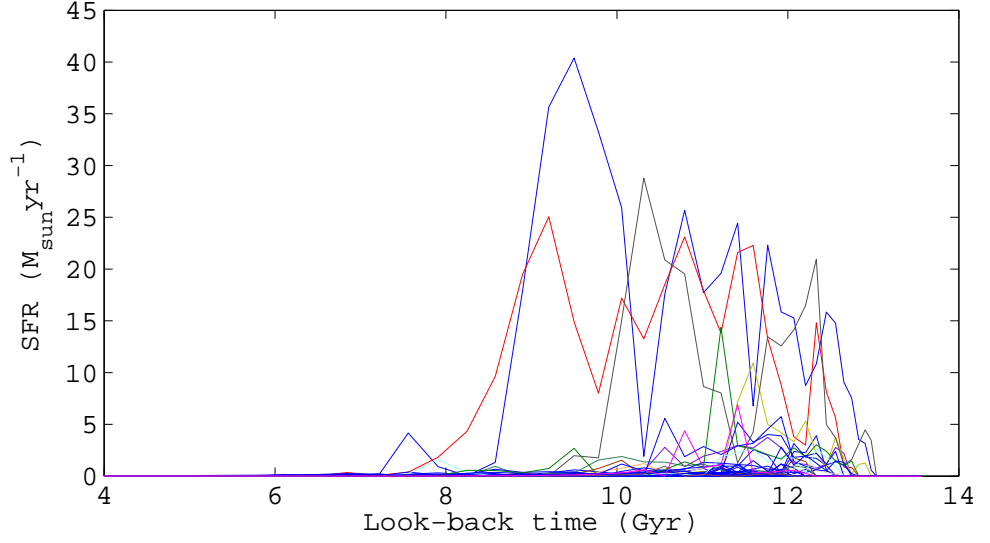


Figure 6: The star formation history for 50 randomly selected model galaxies in the de Lucia et al. model at $z = 0.32$.

and are extended over a longer time interval. Furthermore, less massive LRGs in the Bower et al. model have significant events of star formation. A significant dispersion is shown in formation redshift (z_f), the redshift of peak star formation (z_p), the fraction of galaxies with SFR greater than $5M_{\odot}yr^{-1}$ within one gigayear of the redshift and in the fraction of galaxies with SFR greater than 3σ away from the average SFR. The SFRs, once normalized to the SFR at $z = 0.32$ as in figure 7, show important differences for the two models using the SDSS cuts, there is no monotonic behaviour for successive redshifts. While using the absolute magnitude cuts, only the SFR normalized in the de Lucia model gives a monotonic change from the low to high redshift.

The sample predicted by the Bower et al. using the SDSS cuts seem to be inhomogeneous, but homogeneous using the absolute magnitude cuts. In Bower et al. model, the discussion of the SFR is left for further investigation (Bower et al., 2006).

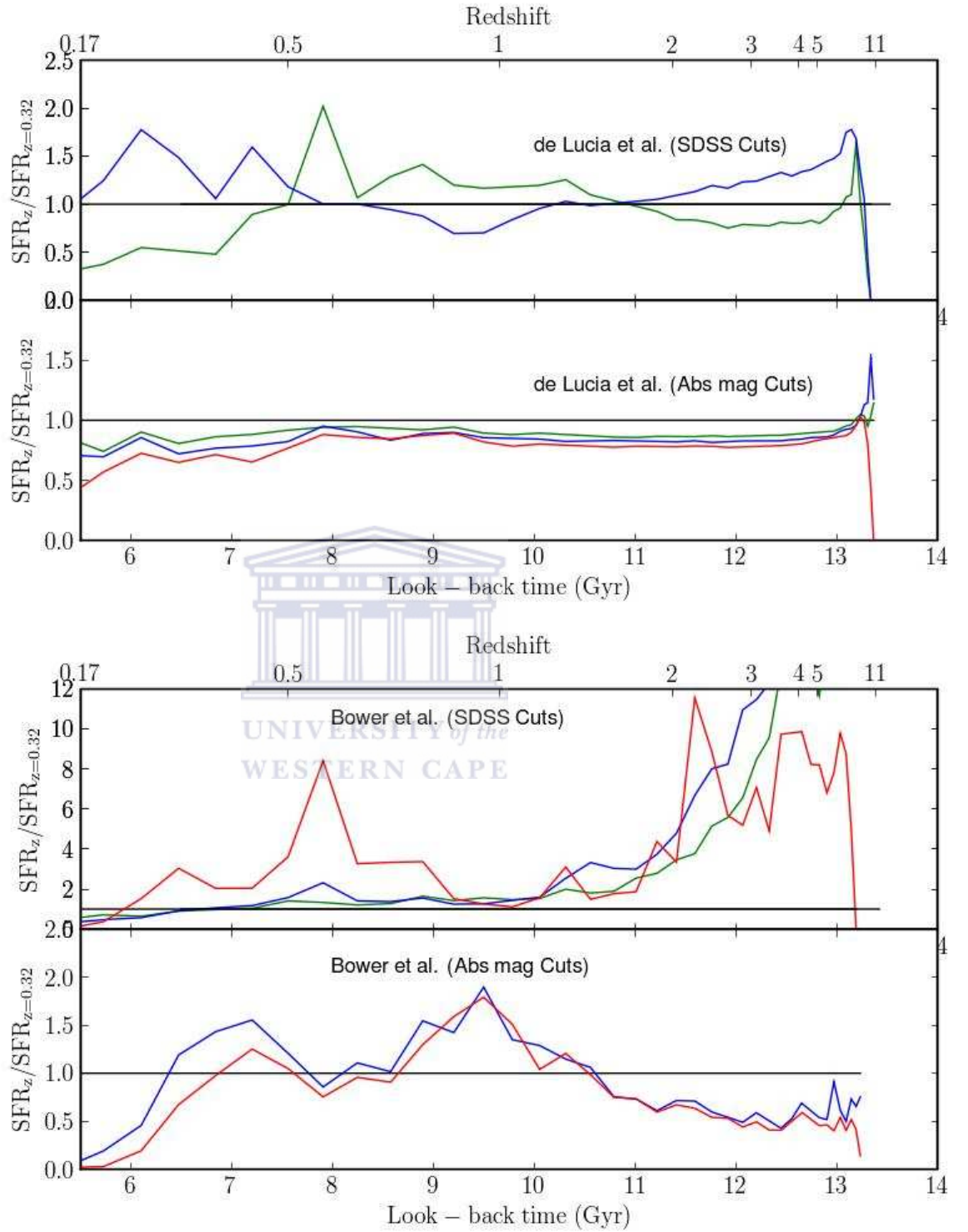
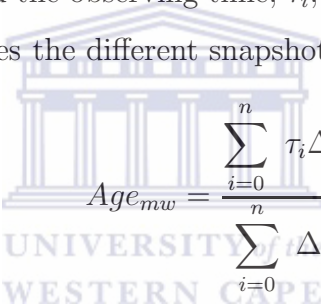


Figure 7: The ratio of the average star formation histories in figure 6 to the average star formation history for the $z = 0.32$ sample. Black lines represent the average SFR at $z = 0.32$; green at $z = 0.46$; blue at $z = 0.51$ and red at $z = 0.56$.

4.3 The distribution of ages of stellar populations and metallicity

The simulation provides mass-weighted ages for the de Lucia et al. model and luminosity weighted ages for the Bower model. The mass-weighted age is defined as the average age of the stars in a galaxy weighted by mass of its components. However, the luminosity weighted age of the stellar population is a measure of the age of the stars weighted by their luminosity; here it is in V-band. To allow comparison between models, we only consider the mass-weighted age. In the Bower et al. model, we compute the mass-weighted age knowing the SFR which is described in the above section. The average age, Age_{mw} , is obtained by dividing the sum of the SFR times the look-back time difference, Δt_i , and the observing time, τ_i , by the total stellar masses of a galaxy. The variable i symbolizes the different snapshots.



$$Age_{mw} = \frac{\sum_{i=0}^n \tau_i \Delta t_i SFR_i}{\sum_{i=0}^n \Delta t_i SFR_i} \quad (40)$$

where $\Delta t_i = t_i - t_{i-1}$ and $\tau_i = t_{obs} - t_i$; here t_{obs} is the time when we observe the galaxy.

The normalized distribution predicted and the calculated mass weighted ages at each redshift of LRGs are plotted in figure 8 in the de Lucia et al. and Bower et al. models respectively. Of these four age distributions, only the age distribution in the de Lucia et al. model using the absolute magnitude cuts shows a significant separation of ages into distinct groups even at very close redshifts, although a small tail of younger galaxies is still present. The distribution of ages is consistent with the idea that most stars in LRGs formed during a 1 Gyr period early in the Universe. It means that they are characterized by the shortest formation time-scales, in agreement with the established down-sizing scenario (Cowie et al., 1996). This is also more consistent with the assumption made by Jimenez et al. (2003) about the formation of these galaxies at the same time. In addition, we can say that LRGs are composed predominantly of old

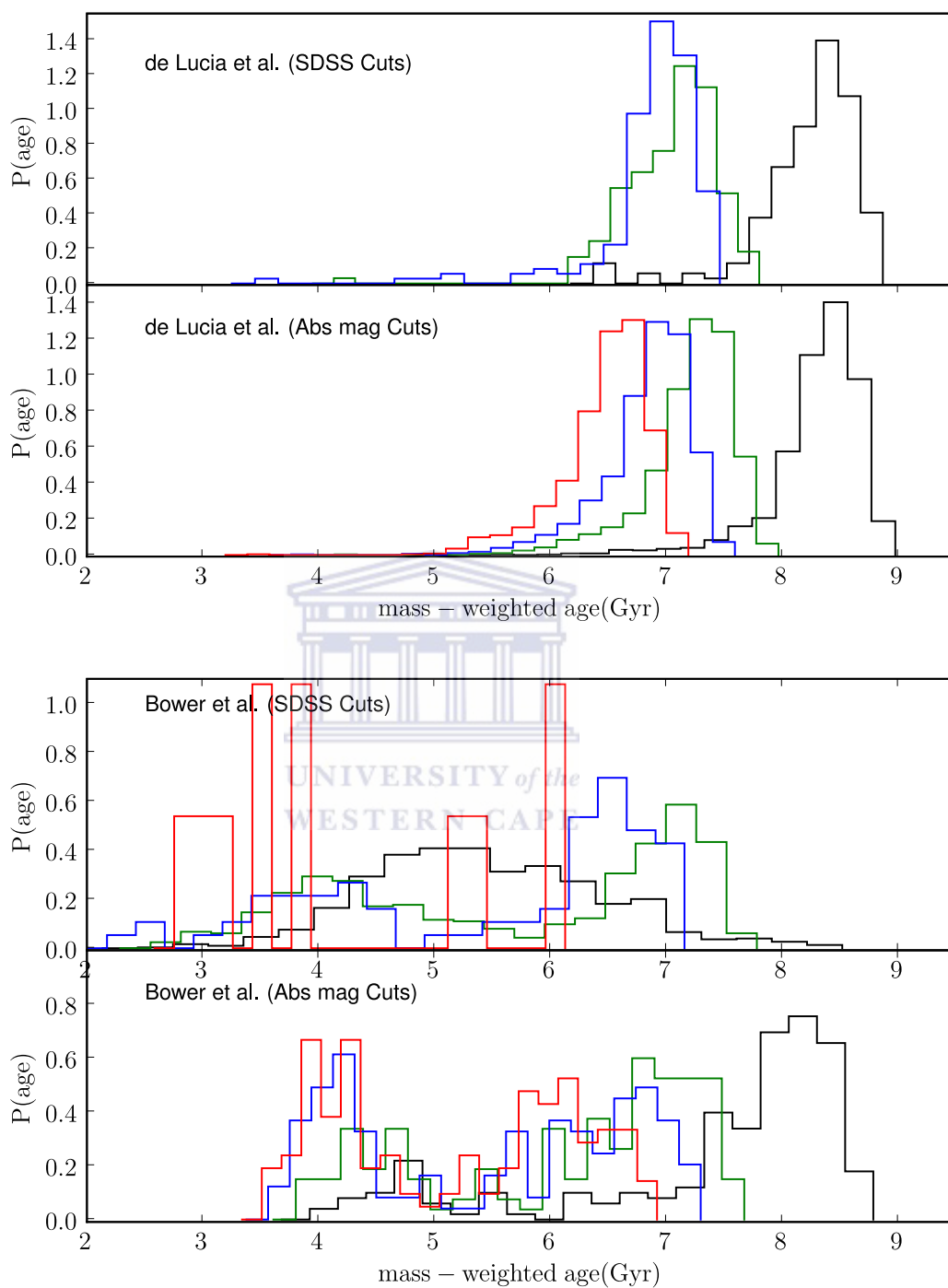


Figure 8: Histogram of the mass-weighted ages at four different redshifts in the two models using the two cuts. Black lines represent the average SFR at $z = 0.32$; green at $z = 0.46$; blue at $z = 0.51$ and red at $z = 0.56$.

stellar populations as in [Trager et al. \(2000\)](#); [Gallazzi et al. \(2006\)](#). In these papers, it is shown that massive LRGs are assembled later than their lower mass counterparts. Our LRG samples have a larger number of progenitor systems, comparing with the randomly selected galaxies which do not show those properties. Note in passing that in hierarchical models, the age of the stellar population in a galaxy probably exceeds the age of the galaxy; that is because stars form in the galaxy's progenitors, which are, in the later snapshots, assembled into the final galaxy through mergers ([Baugh et al., 1996](#); [Kauffmann, 1996](#); [De Lucia and Blaizot, 2007](#)).

Table 5: The comparison between the change of the average mass-weighted age of the LRGs and the change of the age of the Universe Age^a

model	cuts	redshift ranges	ΔAge_u (Gyr)	ΔAge_{mw} (Gyr)
de Lucia et al.	sdss	$z = 0.32-0.46$	1.13	1.27
	sdss	$z = 0.46-0.51$	0.36	0.18
	abs mag	$z = 0.32-0.46$	1.13	1.09
	abs mag	$z = 0.46-0.51$	0.36	0.37
	abs mag	$z = 0.51-0.56$	0.34	0.37
Bower et al.	sdss	$z = 0.32-0.46$	1.13	-0.15
	sdss	$z = 0.46-0.51$	0.36	0.08
	sdss	$z = 0.51-0.56$	0.34	1.27
	abs mag	$z = 0.32-0.46$	1.13	1.28
	abs mag	$z = 0.46-0.51$	0.36	0.62
	abs mag	$z = 0.51-0.56$	0.34	0.33

Notes:

Age_u : the age of the Universe

Age_{mw} : the average mass weighted age of LRGs

Our results disagree with [Kauffmann \(1996\)](#) and [Kauffmann and Charlot \(1998\)](#) about the age of massive elliptical galaxies, they argued that elliptical galaxies are

predicted to show a trend of decreasing age with increasing luminosity, with the brightest ellipticals the youngest, but in agreement with later simulation work (e.g. De Lucia et al., 2006; Almeida et al., 2008). By fitting the spectra of some LRGs from SDSS using stellar population synthesis models, Barber et al. (2007) came up with a range of LRG ages from 4 to 10 Gyr at redshifts in the range $0.15 < z < 0.4$ which matches our mass-weighted age range in the de Lucia et al. model at lower redshift (i.e. at $z < 0.32$). However, LRGs in the Bower et al. model are younger than the ones in the de Lucia et al. model demonstrated by the averages of the mass-weighted ages (Age_{mw}) in table 4; and there is significant scatter in the age distribution using both cuts. Furthermore, older galaxies present a non-gaussian distribution.

Table 5 compares the change in age of the Universe at each redshift with the change in Age_{mw} . If we assume that LRGs are passively evolving, then the change in their age with redshift should correspond to the change in the age of the Universe (Age_u). Again, only LRG's age differences in the de Lucia et al. model extracted using absolute magnitude cuts correspond more or less to the Universe's age differences with ~ 0.03 Gyr uncertainty. The difference in the ages predicted by the de Lucia et al. and Bower et al. models has its origins in the different implementations of gas cooling and feedback applied in massive dark matter haloes. De Lucia et al. (2006) show that the suppression of gas cooling due to AGN feedback tends to increase the gas of the stellar population in the galaxies hosted by haloes with quasi-static hot gas atmospheres.

Regarding the metallicity of LRGs; the comparison of the metallicity distributions with the mass-weighted ages of modeled galaxies is shown in figure 9. In the de Lucia et al. model we calculate the metallicity of these galaxies by taking the metallicity of cold gas out of which these galaxies are formed. If the interstellar gas has a mass M_g and contains a mass of heavy elements M_h , the metallicity of the galaxy is then

$$Z = \frac{M_h}{M_g} \quad (41)$$

The metallicity is ranging from $0.25Z_\odot$ to $3Z_\odot$, and its distribution peaks at solar metallicity. We use this metallicity and SFR as an input to generate the LRG spectra

in the next chapter. However, the V-band luminosity weighted metallicities for LRGs are given for the Bower et al. model, so direct comparison with the de Lucia et al. model is difficult. The upper limit of the range of luminosity weighted metallicity for LRGs in this model decreases by a factor almost 2.5. Concentrating on using the absolute magnitude cuts, the metallicity in the de Lucia et al. model does not change with redshift while in the Bower et al. model, it increases with redshift. In reality, the possible explanation of this phenomenon is at low redshifts, we effectively pick a large number of brighter and probably older objects, since we have not taken passive evolution into account in the cuts. Although there is a significant scatter in the metallicity against the mass-weighted age using both cuts; and a big change between the samples from the two models. This difference is presumably due to the choice of IMF used in the models and also feedback prescriptions. As mentioned in the previous chapter, de Lucia et al. considered that stars form from the cold disk gas or in a burst with a [Kennicutt \(1983\)](#) IMF, whereas in the Bower et al. model, a [Chabrier \(2003\)](#) IMF is adopted in all modes of star formation. [Barber et al. \(2007\)](#) presented high metallicities in their sample and best fits to the spectra of SDSS LRGs in the range $-0.4 < [Z/H] < 0.4$. They argue that this is evidence in favour of LRGs-forming stars with a top-heavy IMF.

4.4 Stellar mass

We plot in figure 10 the predicted stellar masses of LRGs in the models. These galaxies display large stellar masses as we expected from their high luminosities. The range in stellar masses and their median at each redshift are summarized in table 6. The two models almost agree on the value of the median stellar mass. The masses are found to lie predominantly in narrow range within $10^{11} < (M_*/M_\odot) < 10^{12}$ which is in remarkably good agreement with the masses found observationally by [Barber et al. \(2007\)](#) at $z < 0.4$ with the median stellar mass of $\log_{10}(M_*/M_\odot) = 11.49$. This narrow range of LRG masses confirm our LRG samples have yielded the most massive populations in simulation. No tight correlation is found in the age versus mass. The

distribution clearly does spread towards the old and massive galaxies. We do not consider any evolution correction on the different selection criteria but the models predict the LRG stellar mass to change by a factor of ~ 1.6 between the $z = 0.56$ and 0.32 samples. As mentioned by [Almeida et al. \(2008\)](#), the stellar mass is a robust prediction which is not very sensitive to the details of the implementation of the physics ingredients of galaxy formation.

4.5 Dark halo mass

We have already shown in figure 10 that LRGs tend to be the most massive galaxies in the simulation at a given redshift. We therefore expect them to be hosted by the most massive dark matter haloes present at a given snapshot. We note here that in practice, the efficiency of galaxy formation tends to drop with increasing halo mass, as proved observationally by an increase in the mass to light ratio in clusters compared with galactic haloes ([Eke, 2004](#)). Furthermore, in hierarchical structure formation, the formation histories of galaxies found in the deepest gravitational potential wells are shifted to earlier times compared with galaxies of the same mass found in less extreme haloes. The most massive haloes will tend to be found in regions with higher overdensity. The two models predict which dark matter haloes contain LRGs. Figure 11 shows how the distribution of the halo masses hosting LRGs depends on their mass-weighted ages. Each model demonstrates a different scatter of the halo mass distributions, this could be due to differences in how halo masses are calculated. In the de Lucia et al. model, using the SDSS cuts and absolute magnitude cuts, we note that the more massive haloes contain older galaxies, a correlation which arises naturally in hierarchical structure scenarios and corresponds to the observed phenomenon of downsizing. However, this trend is not present in the Bower et al. model: a big spread of the halo mass distribution due to the number of young galaxies; a significant number of LRGs hosted in less massive haloes; LRGs in this model tend to occupy haloes with a broader mass range than in the de Lucia et al. model from $10^{12} - 10^{15} h^{-1} M_{\odot}$ which is a large range compared to the effective halo mass ($10^{13.61} - 10^{13.80} h^{-1} M_{\odot}$ at $0.4 < z < 0.7$) found

by [Blake et al. \(2008\)](#) by analyzing the small scale clustering of megaZ-LRG based on the SDSS LRG photometric-redshift catalogue, but not far from the halo mass range $10^{13} - 10^{14} h^{-1} M_{\odot}$ given by [Zheng et al. \(2008\)](#) by performing Halo Occupation Distribution (HOD) modelling to interpret small scale and intermediate scale clustering of SDSS LRGs.

4.6 Colours of simulated LRGs

Semi-analytical models track the amount of light of model galaxies. Since the SDSS cuts are based on g-r and r-i colours and the absolute magnitude cuts on B-V colour in rest frame, we looked at how the colour distributions of LRGs depend on their mass-weighted ages. [Figure 12](#) shows the predicted colour distributions of LRGs using the two cuts. We do not find any tight correlations between the ages and the colours. But the scatter of the distribution is due to the abundance of young populations particularly in the Bower et al. model.

4.7 Morphology of LRGs

The morphological type of a galaxy describes its physical appearance or its structural properties; it provides information on the processes that shaped it and probably continue to affect its evolution. To describe the morphology of typical LRGs, we follow the method often used by previous works in semi-analytical models (e.g [Baugh et al., 1996](#); [De Lucia et al., 2006](#)) based on the bulge to total luminosity ratio (B/T). We use this ratio measured in the rest frame B-band ($R = L_{B,bulge}/L_{B,total}$) to apply a morphological classification to the model galaxies. Several observational and theoretical studies have examined images in different bands to make morphological classifications. This ratio corresponds to the bulge to total luminosity ratio observational indicators of morphology by [Simien and de Vaucouleurs \(1986\)](#), based on the identification of features such as spiral arms and galactic bars. We know by definition that LRGs are luminous ellipticals but it is useful to verify the morphology of predicted LRGs in

Λ CDM. Galaxies are classified as ellipticals if $R < 0.4$; galaxies with $R > 1.56$ correspond approximately to the late-type or spiral galaxies, those with intermediate value $0.4 < R < 1.56$ correspond to lenticulars. We note that the classification of irregular and interacting galaxies is not suitable in the B-T definition.

We plot the predicted distribution of the bulge to total ratio in B-band in figure 13 in the two models, using the absolute magnitude cuts only. The results are also summarized in table 7. All samples are mainly composed of bulge-dominated galaxies with up to $\sim 90\%$ of the LRG population in the de Lucia et al. model and $\sim 80\%$ in the Bower et al. model and a few late-type and lenticular galaxies. The two models differ in the intermediate B/T ratio range which corresponds to the SO types or lenticular galaxies. This difference is the result of the interplay between several phenomena such as the mechanism for making spheroids from the rearrangement of stellar disks or through triggering additional star formation. The de Lucia et al and Bower et al. models both consider starbursts from disks dynamically unstable to bar formation, bursts driven by galaxy mergers, but they differ on the determination of the merger timescales on partial versus entire collapse of the disk in modelling the bar formation, and the mass fraction of the cold gas resulting from the merger of two galaxies.

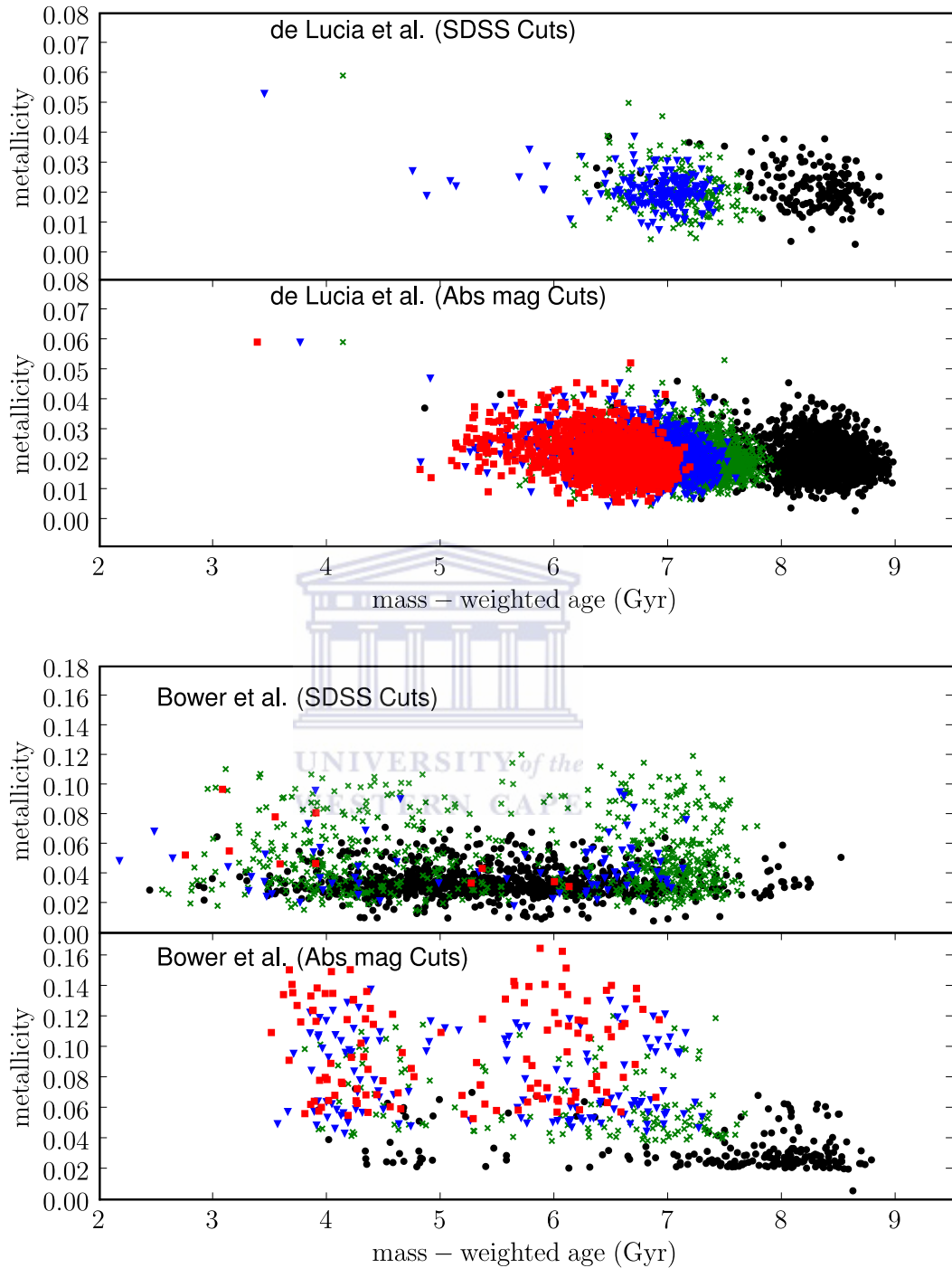


Figure 9: Metallicity distribution of LRGs at four different redshifts in the two models using the two cuts. Black filled dots represent the average SFR at $z = 0.32$; green stars at $z = 0.46$; blue diamonds at $z = 0.51$ and red squares at $z = 0.56$. *Notes:* in the de Lucia et al. model, we extracted the metallicity of the cold gas out of which LRGs are formed, however in the Bower et al. model, we extracted the luminosity weighted metallicity.

Table 6: The stellar masses range and its median for each redshift bin in the models.

model	cuts	redshift	Stellar masses range ($10^{11}h^{-1}M_{\odot}$)	median ($10^{11}h^{-1}M_{\odot}$)
de Lucia et al.	sdss	0.32	2.00 - 7.81	2.97
	sdss	0.46	2.00 - 4.92	2.57
	sdss	0.51	1.56 - 6.73	3.64
	abs mag	0.32	1.72 - 12.42	3.10
	abs mag	0.46	1.80 - 9.04	2.75
	abs mag	0.51	1.66 - 8.46	2.63
	abs mag	0.56	1.73 - 8.18	2.50
	Bower et al.	sdss	0.32	0.69 - 3.98
sdss		0.46	0.87 - 7.44	2.50
sdss		0.51	1.20 - 7.19	3.64
sdss		0.56	1.20 - 7.18	2.24
abs mag		0.32	1.90 - 7.22	3.31
abs mag		0.46	1.90 - 5.12	2.86
abs mag		0.51	1.85 - 4.69	2.64
abs mag		0.56	1.83 - 4.69	2.55

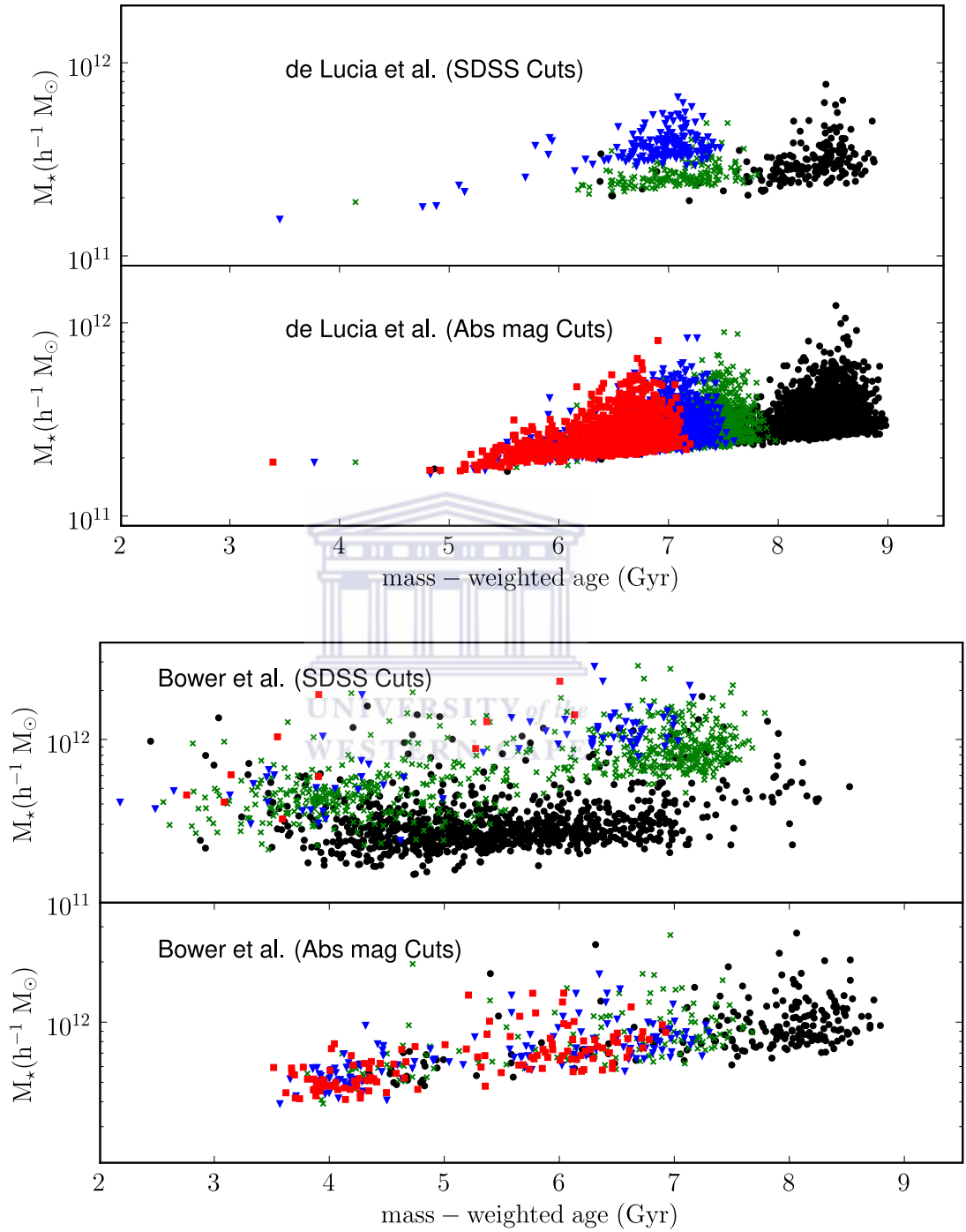


Figure 10: Stellar masses distribution of LRGs at four different redshifts in the two models using the two cuts. Black filled dots represent the average SFR at $z = 0.32$; green stars at $z = 0.46$; blue diamonds at $z = 0.51$ and red squares at $z = 0.56$.

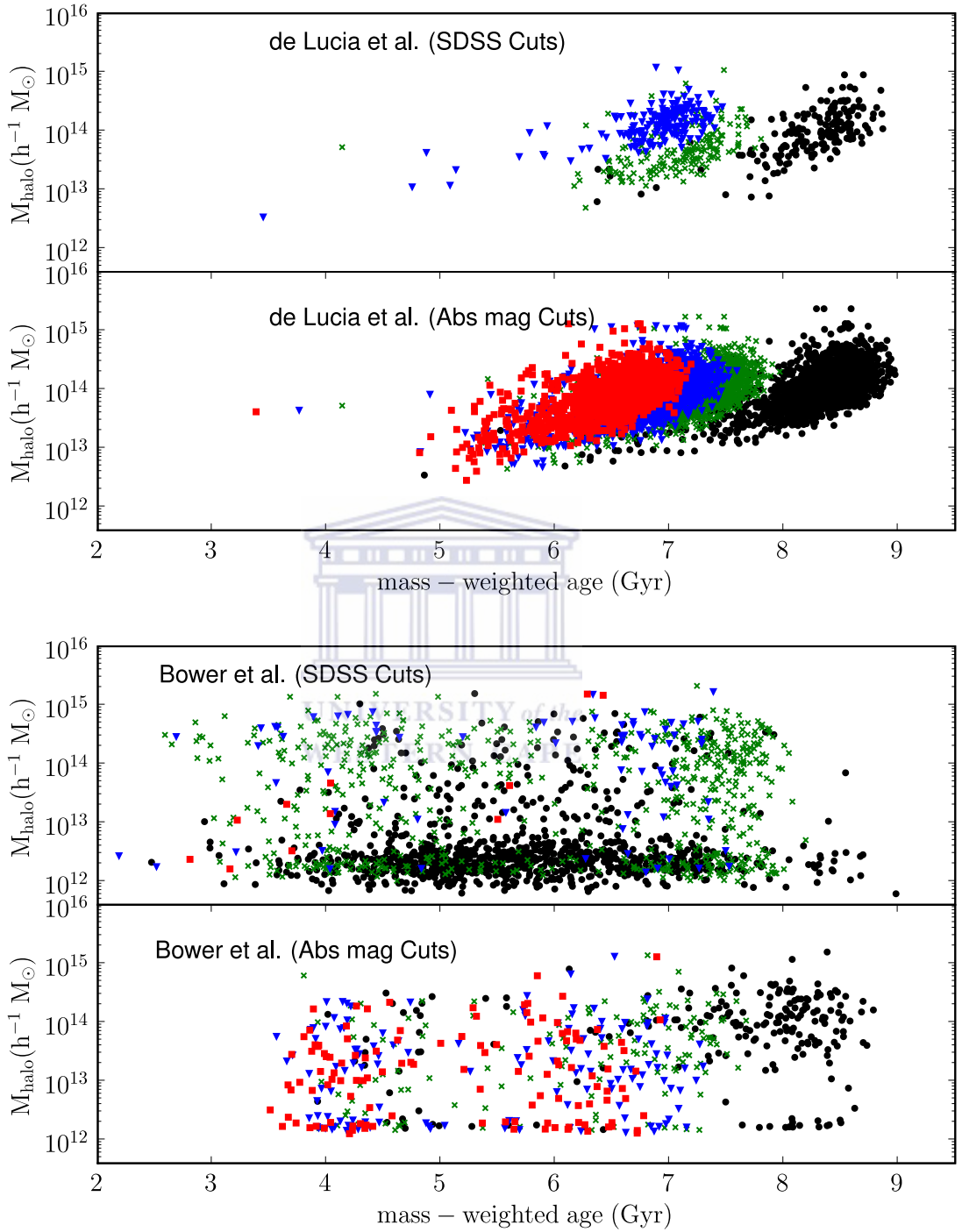


Figure 11: Distribution of dark halo masses hosting LRGs at four different redshifts in the two models using the two cuts. Black filled dots represent the average SFR at $z = 0.32$; green stars at $z = 0.46$; blue diamonds at $z = 0.51$ and red squares at $z = 0.56$.

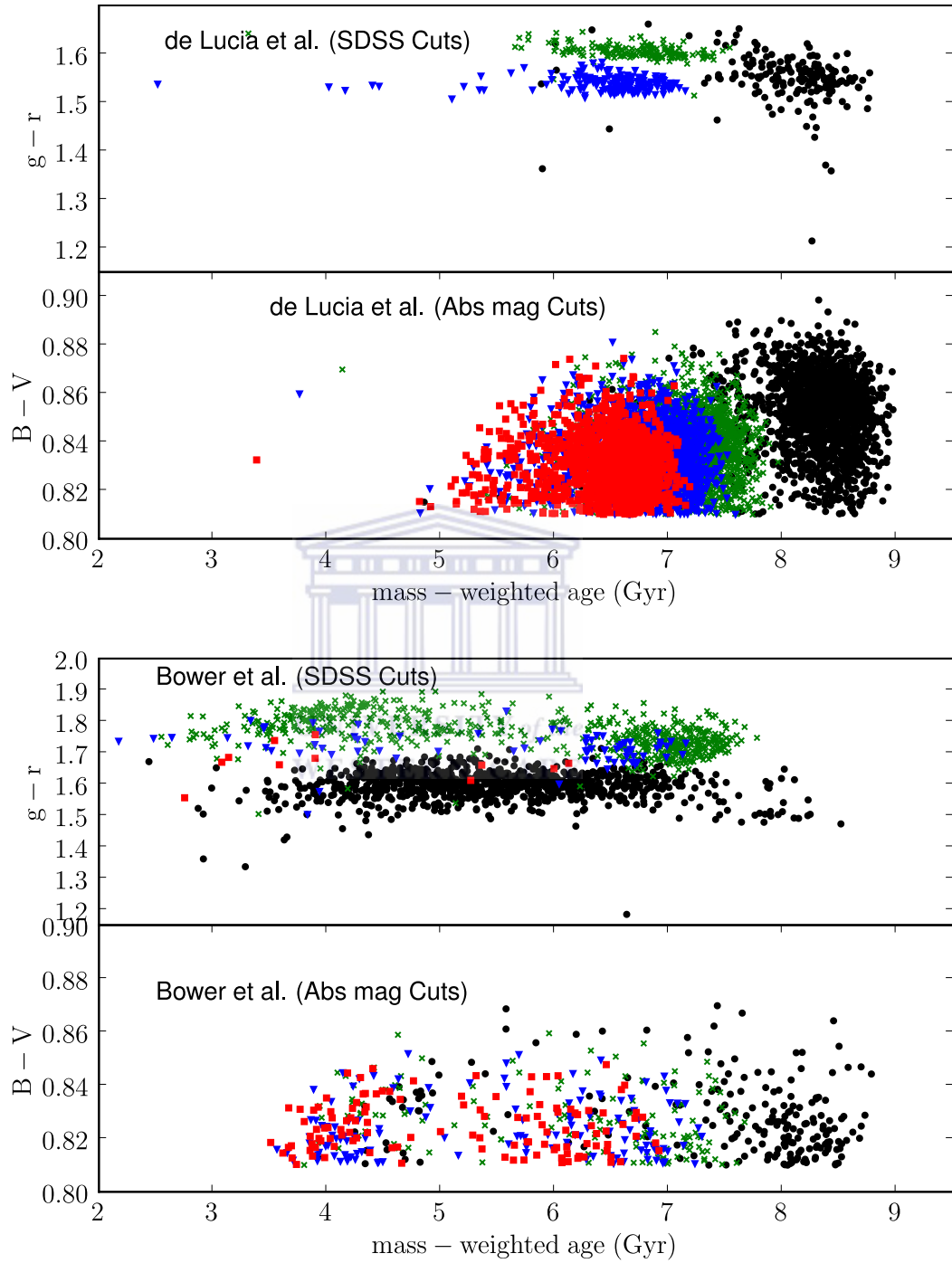


Figure 12: Colour distribution of LRGs at four different redshifts in the two models using the two cuts. Black filled dots represent the average SFR at $z = 0.32$; green stars at $z = 0.46$; blue diamonds at $z = 0.51$ and red squares at $z = 0.56$.

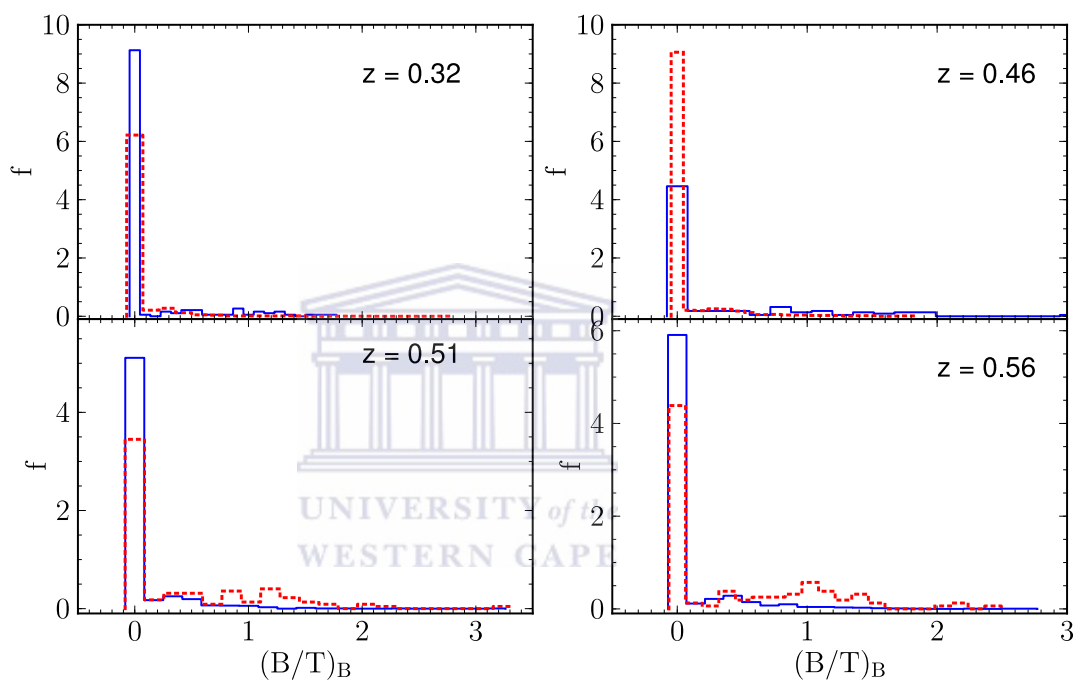


Figure 13: The predicted morphological mix of LRGs in the two models at four different redshift bins. Red dashed lines represent galaxies from the de Lucia et al. model, whereas blue solid lines from Bower et al. model using the absolute magnitude cuts. f is the number of galaxies normalized.

Table 7: The predicted morphological mix of LRGs at different redshifts in the two models.

model	redshift	$R < 0.4$	$0.4 < R < 1.56$	$R > 1.56$
de Lucia et al.	0.32	1623	77	5
	0.46	1372	116	3
	0.51	1300	142	6
	0.56	1181	147	9
Bower et al.	0.32	177	27	3
	0.46	104	25	9
	0.51	84	38	9
	0.56	72	45	6

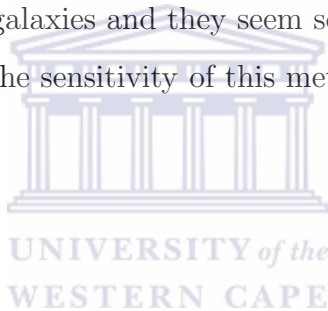
4.8 Summary



We have investigated the properties of LRGs in the Λ CDM cosmology using two galaxy formation models based on the Millinium simulation, one by de Lucia et al. (the MPA model) and the other by Bower et al. (the Durham model). As we have seen in chapter 2, there are some difference between the input physics, model ingredients and parameters choices in the two models. Both models have had remarkable success in producing a number of observed properties of the local and high redshift universe, including star formation, stellar masses and many others properties. Here, there are certain similarities but also disagreements in the predictions of the star formation rates and other properties of the predicted LRGs using the similar selection criteria. Starting from the abundance of LRGs in samples using two cuts, only the de Lucia et al. model, when absolute magnitude cuts are applied, have given us a large sample of LRGs with number densities at $z = 0.51$ close to the observed values and SFHs suitable for the age-dating experiment i.e, the mass-weighted age distribution shows a strong peak at a single age; the change of the average ages is consistent with the change of the age of the

Universe; and lower percentage of galaxies showing any star formation since $z \sim 1.7$. It appears that these galaxies can be used as a cosmic chronometers to recover the cosmology used in the MS.

The samples selected using SDSS cuts either in the de Lucia et al. or in the Bower et al. model are not very homogeneous. The selection of galaxies in apparent magnitude space causes this inhomogeneity. Due to the width of the redshift bin within which the apparent colour cuts are defined, we probably have selected a large number of galaxies that have more extended SFH. In addition, in the Bower et al. model, using the absolute magnitude cuts we have selected a large number of young LRGs even though the change in their age with redshift does roughly correspond to the change of the Universe's age. This is due to the fact that the Bower et al. (2006) model simulated a small amount of red galaxies and they seem so young. Inclusion of these last galaxy samples may decrease the sensitivity of this method of $H(z)$ measurement.



Chapter 5

5 Recovering $H(z)$



In this chapter I explore the uncertainties on the Hubble parameter, $H(z)$, related to the extended star formation histories of LRGs and ignore the difficulties associated with measuring the age of LRGs. As mentioned in the summary part of the previous chapter, we focus only on the LRG samples extracted in the de Lucia et al. model using the absolute magnitude cuts. Here we use the mass-weighted ages plotted in the second panel of figure 8 for galaxies in the four redshifts initially used.

5.1 Method

To determine the accuracy with which $H(z)$ can be measured, we need to extract galaxies from larger range of snapshots in the redshift range $0 < z < 1$. We have adjusted our colour cuts relative to $z = 0.51$ to account for passive evolution. The distribution of mass-weighted ages of LRGs selected here are similar to those discussed in chapter 4. We compare three different methods to determine the characteristic age of LRGs at a given redshift:

- a) calculating the average of the ages,
- b) fitting a function to the distribution of ages, and
- c) matching pairs of galaxies.

For each method, we calculate $H(z)$ using its definition:

$$H(z) = -\frac{1}{1+z} \frac{dz}{dt} \approx -\frac{1}{1+z} \frac{\Delta z}{\Delta t}. \quad (42)$$

By Jimenez and Loeb (2002), the $H(z)$ is determined by the measurement of the age difference, Δt between two LRG populations separated by a small redshift interval Δz . If we assume no error in the redshift, the error in $H(z)$ will only depend on the age at t_1 and t_2 (where $\Delta t = t_1 - t_2$):

$$\frac{\sigma_H^2}{H(z)^2} = \frac{(\sigma_{t1}^2 + \sigma_{t2}^2)}{(t_1 - t_2)^2}. \quad (43)$$

Figure 14 presents the $H(z)$ estimates using the three methods given above. We plot the difference between our calculated value $\Delta z/\Delta t$, and the expected value for $H(z)$

based on the equation (3) in [Jimenez and Loeb \(2002\)](#):

$$-(1+z)\frac{H(z)}{H_0} = -(1+z)^{5/2} \left\{ \Omega_m(0) + \Omega_Q(0) \times \exp \left[3 \int_0^z \frac{dz'}{1+z'} w_Q \right] \right\}^{1/2}, \quad (44)$$

where $w_Q = P_Q/\rho_Q$ is the equation of state parameter for the dark energy and in the Λ CDM of the de Lucia et al. model, $w_Q = -1$.

5.2 Results

As we see in figure 14, $H(z)$ is fairly well recovered by using the average method (top panel). If we assume an error in the mean age at a specific redshift of 0.03 Gyr (this error will be discussed later in next chapter), then $H(z)$ can be calculated to a precision of 1.6% at $z \approx 0.42$ using the redshift interval between $z = 0.32$ and $z = 0.51$. The smaller the redshift interval, the larger the error on $H(z)$. Since the error in $H(z)$ is inversely proportional to the difference in age as seen in equation 43. Between $z = 0.51$ and $z = 0.56$, a small systematic error in mean age of 0.5% will result in the calculation of $H(z)$ to be off by 10%. The curvature of $H(z)$ over these redshift ranges is small thus we can use large values of Δz and not affect the value of $H(z)$.

With the method of fitting a function to the distribution of the ages to determine a characteristic age (the middle panel), $H(z)$ is slightly underestimated at the highest redshifts. Our mass weighted-age distribution was fitted to the following function:

$$P(t) = \frac{a \times g(t)^2}{1 + g(t)^b}, \quad (45)$$

where $g(t)$ is defined as:

$$g(t) = \frac{t_0 - t}{c}. \quad (46)$$

This fitting method is similar to fitting the envelope of oldest galaxies in [Jimenez et al. \(2003\)](#). For the first test, we allowed the parameters a , b , and c to be free along with t_0 . In the second test, we varied the two parameters b and c to 5.52 and 0.66 respectively, which were the average parameters found during the free fits, and solved for a from the best fit value of t_0 . The free and fixed fits showed a similar result for $H(z)$. The

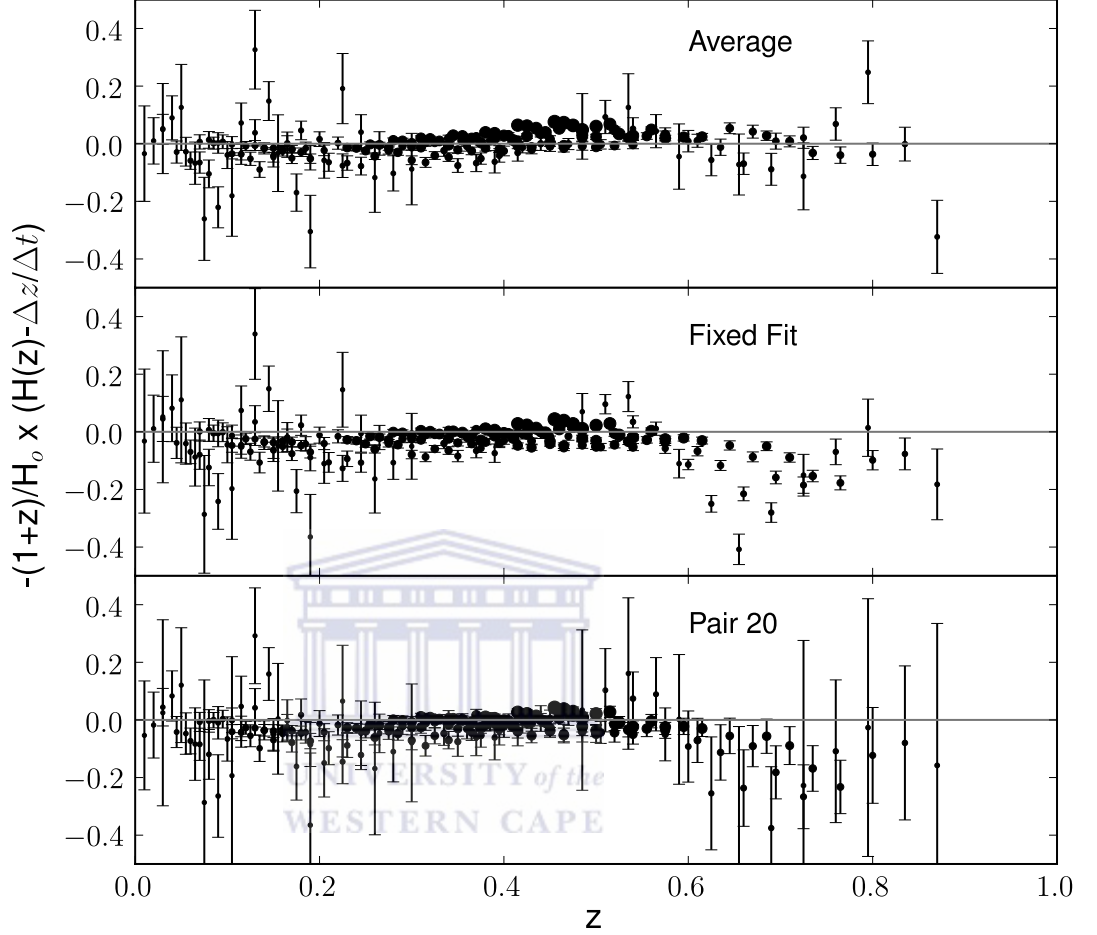
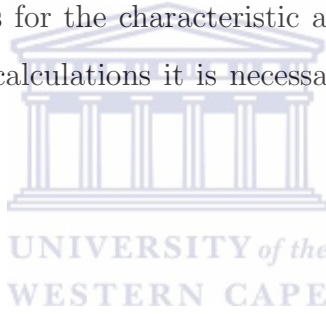


Figure 14: The difference between $H(z)$ and $\frac{\Delta z}{\Delta t}$ calculated from the Average (top), Fixed fit (middle), and Pair 20 (bottom) methods. The size of each point is related to the distance between the redshift snapshots which range from $\Delta z = 0.02 - 0.91$. Larger errors are typically associated with smaller redshifts intervals.

middle panel shows the result obtained with the fixed fit. The shift at highest redshifts is probably due to the fitting function being less appropriate at higher redshift. At $z \approx 0.42$, we obtained a calculation of $H(z)$ to 1.1% precision using the redshift interval between $z = 0.32$ and $z = 0.51$.

The last method consists of calculating $H(z)$ at a given redshift based on the distribution of $H(z)$ calculated between each pair of galaxies in the redshift bins. To avoid the overlap between the age distribution by using the whole sample, we picked the 1000 oldest galaxies because, using less than 10 galaxies results in anomalous values of $H(z)$, whereas using the 20 oldest galaxies minimizes both the systematic and random errors on the calculation of $H(z)$. Once we have calculated the value of $H(z)$ from all pairs, $H(z)$ at a given redshift is the three-sigma clipped mean of the distribution. The error is then given by the standard deviation of the sigma-clipped distribution. Similar to the result by using the second method, the $H(z)$ calculated is also slightly below the model but well within the errors. At $z \approx 0.42$ $H(z)$ can be calculated to 2.8% precision. From these results, we can conclude that we are able to recover $H(z)$ at a single redshift using different methods for the characteristic age of the population. To estimate the uncertainties on $H(z)$ calculations it is necessary to use simulations where the SFHs are known.



Chapter 6

6 Simulated Spectra of LRGs



In this chapter I describe how we simulated the LRG spectra using spectral synthesis models. As mentioned earlier in chapter 4, we use the SFR and metallicity of model LRGs extracted from the de Lucia et al. model using the appropriate cuts (absolute magnitude cuts), to generate the simulated spectra of these galaxies. There are many stellar population synthesis codes available to generate galaxy spectra using a determined star formation history (e.g [Fioc and Rocca-Volmerange, 1997](#); [Bruzual and Charlot, 2003](#)). The composition of each code is different. Stellar population models require understanding of the photospheric emission from stars in galaxies and star clusters. The theoretical stellar population models do not perfectly reproduce real stars at all wavelength ranges (e.g [Bertone et al., 2008](#)), but the replacement of the optical wavelength part of the theoretical stellar spectra with spectra derived from empirical spectral libraries might be a solution for such problem ([Walcher et al., 2009](#)). To start with, the U-UV spectral range is not well produced, and an excess U flux is seen in typical galaxy SEDs ([Walcher, 2008](#)). In the NIR spectral range study, AGB and Thermally-Pulsating Asymptotic Giant Branch stars (TP-AGB) are apparently more numerous, brighter and redder than originally thought and contribute 60 % of the K-band light in the galaxy rest-frame, i.e. they tend to dominate the integrated light of old stellar populations, implying less mass to produce M_*/L (e.g [Maraston, 2005](#)). An evolving IMF might be required to model cluster red-sequence galaxies which include many LRGs ([van Dokkum, 2008](#)) (we have not included that in our model). Related to the IMF, the alpha-element enhancement of massive and old galaxies is not correctly modelled ([Walcher et al., 2009](#)). Blue stragglers and blue horizontal branch morphologies can also affect (in age-dependent fashion) the SEDs (Spectral Energy Distributions) and derived properties of passive galaxies. Moreover, the treatment of non-solar abundance ratios in population synthesis models can affect stellar ages of early-type galaxies derived from spectral features (e.g [Thomas et al., 2004](#)). Finally, dust modelling remains uncertain. Many recent models have been tested and developed (e.g [Maraston, 2005](#); [Maraston et al., 2009](#); [Conroy et al., 2009](#)) along with improvements in the underlying stellar evolution models ([Marigo et al., 2008](#)). Furthermore, there is still uncertainty in the best method for deriving accurate ages at low redshift

(Kannappan and Gawiser, 2007; Wolf et al., 2007; Trager and Somerville, 2009) and at high redshift (Longhetti and Saracco, 2009; Maraston et al., 2009; Muzzin et al., 2009). In passing, improvements in constant IMFs in the last decade have been made (Kroupa, 2001; Chabrier, 2003), but most recent works have invoked an evolving IMF (Fardal et al., 2007; Davé, 2008; van Dokkum, 2008) where the characteristic mass shifts towards higher values at higher redshifts.

6.1 Stellar population synthesis models

Here we carry out a study of the age-dating using the BC03 model. We give an overview of this model and how we model the LRG spectra and age-date the simulated spectra. Despite the many uncertainties in the spectral synthesis models, they do provide a first order approximation to real spectra.

The BC03 is a high spectral resolution stellar evolutionary synthesis model produced by Bruzual and Charlot (2003) in which a library of single stellar populations (SSPs) is incorporated. The BC03 library has been employed by several researchers to decompose galaxy spectra into various SSPs of different ages and metallicities. This model is used to compute the spectral evolution of stellar populations at the following range of ages : 1×10^5 to 2×10^{10} years at a resolution of 3 \AA across the whole wavelength range from 3200 to 9500 \AA for a wide range of metallicities ($Z = 0.0001Z_{\odot}$ to $Z = 0.05Z_{\odot}$), and at lower resolution from 91 \AA to $160\mu m$. The predictions of this library are based on the observed spectra (Le Borgne et al., 2003). The model reproduce well the observed optical and near infrared colour-magnitude diagrams of Galactic star clusters of various ages and metallicities. They note that the full range of observed integrated colours of star clusters in the Magellanic clouds can be accounted for by stochastic fluctuations in the number of stars in different evolutionary phases. A prescription for TP-AGB is included in the BC03 which is supported by observations of surface brightness fluctuations in nearby stellar populations. This model is the first to produce accurate absorption-line strengths in galaxies containing stars over the full range of ages. In this study, we are using the optical regime to look at much older galaxies,

where the effects of the TP-AGB stars are expected to be minimal.

6.2 Modelling LRG spectra

We use the BC03 model to generate LRG spectra. We produce spectra of LRGs by combining SSP spectral libraries of BC03. We have assumed the standard Salpeter IMF with mass cut-offs at 0.1 and $100M_{\odot}$. As demonstrated in chapter 3 we are in possession of both star formation rate and metallicity of the cold gas out of which the stars are formed as a function of time. Using these two parameters and SSP spectral libraries as input, we calculate the emergent spectrum according to

$$F(\lambda) = \int_0^{t_{form}} S(t) F_{SSP}(\lambda, t, Z(t)) dt, \quad (47)$$

where $F(\lambda)$ is the emergent spectrum in the rest frame, t the look-back time at the start of formation, $S(t)$ the SFR per unit mass per unit time, $F_{SSP}(\lambda, t, Z(t))$ the spectrum of an SSP as a function of age and metallicity normalized to unit mass of stars; $Z(t)$ is the metallicity as a function of look-back time; and λ is the wavelength. We ignore the effect of dust, since these LRGs are assumed to be red and dead thus containing little dust (Barber et al., 2007). Note that the look-back time is the time between the snapshot (typically, we extract galaxies at snapshots corresponding to $z \sim 0.5$) and the redshift at which star formation occurs.

We generate spectra for all LRG samples in the De Lucia et al. model using the absolute magnitude cuts at four different redshifts. We consider in particular the $z = 0.51$ galaxies to examine the limitations in age-dating the stellar populations. Figure 15 presents the average spectrum of the first 200 luminous red galaxies extracted from SDSS catalogue which satisfied our absolute magnitude cuts; and the best fit model spectrum at $z = 0.46$ using the SFH and the metallicity of simulated galaxies as a function of time. The fit was made from 3500 – 6000 Å which includes only the high-resolution portion of the models. The best fit model has a mass-weighted age of 7.11 Gyrs. The overall shape of the model is in good agreement with the observed spectrum although there are some inconsistencies at the long and short wavelength ends.

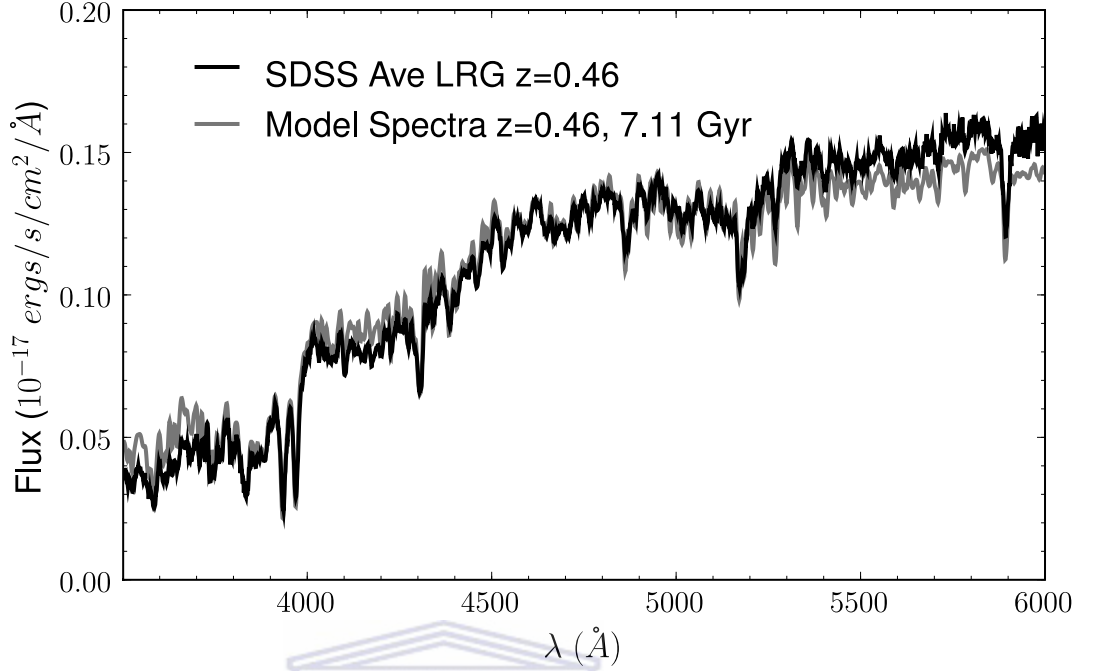


Figure 15: Average spectrum of 200 SDSS LRGs from galaxies at $z = 0.46$ satisfying the absolute magnitude cuts, compared to the best-fit model spectrum produced using the BC03 model with the SFH and metallicity from the MS at $z = 0.46$. The spectrum is normalized to observed values at 4130 \AA .

6.3 Age-dating simulated LRG spectra with SSPs

In our first attempt at age-dating the LRG spectra, we used the SSP template library of BC03. We determined the ages of 1448 model LRGs at $z = 0.51$ without introducing any flux errors. For each source we fitted the full spectra from $\lambda = 3500 - 9000 \text{ \AA}$ using the SSP library described in §6.1. We then determined the best fit by minimizing the χ^2 .

In table 8, for our entire sample we show the results of the age-dating including the systematic and random errors from fitting with SSPs. The systematic errors (Δ^b) are obtained by comparing the mean of the measured ages using SSPs and the mass-weighted ages, whereas the random errors (σ^c) are the standard deviation of the difference between these measured ages and the mass-weighted ages. The re-

Table 8: Errors from age-dating. Comparison between ages and errors in ages from SSP fitting and from fitting with our model spectra.

z	SSP Fit				Model Fit		
	age_u	age	Δ^b	σ^c	age	Δ^b	σ^c
0.32	10.08	8.15	0.14	1.85	8.32	0.01	0.29
0.46	8.95	7.42	0.20	1.72	7.22	0.01	0.33
0.51	8.59	7.06	0.23	1.65	6.83	0.02	0.33
0.56	8.25	6.62	0.16	1.69	6.48	0.01	0.33

Notes:

age_u Age of the Universe in Gyrs.

^b Mean difference between measured age and mass-weighted age.

^c Standard deviation of difference between measured age and mass-weighted age.

sult of the systematic errors in the age determination is not surprising, as given in [Trager and Somerville \(2009\)](#): by comparing the observed and simulated populations with SSPs, they also find that the SSPs underestimate the age of red galaxies in the Coma cluster and it is poorly correlated with the mass-weighted age, this is caused by the SSPs being dominated by recent star formation. According to [Jimenez et al. \(2004\)](#) the differential ages are less sensitive to the systematic errors, and if the systematic errors were constant, this would not affect the calculation of $H(z)$. Since our systematic errors change with redshift, we are not able to rely on the SSP-calculated ages to determine $H(z)$.

To investigate the effects of changing the SNR and resolution of spectra on calculating the age of LRGs, we performed a Monte Carlo simulation for a subset of 10 randomly selected galaxy spectra from our sample at $z = 0.51$. The template library and the spectra were convolved to a resolution of $\Delta\lambda = 3, 5, 10, 20 \text{ \AA}$. We then added noise to each spectra giving a range of signal to noise (SNR) from $SNR = 3, 5, 10, 30, 50, 100, 200$. We define the SNR here as the average SNR per resolution element of the spectrum between 3000 and 9000 \AA assuming simple shot noise. χ^2 minimization was used to find the metallicity, age and normalization of the best fitting SSP spectrum. For each

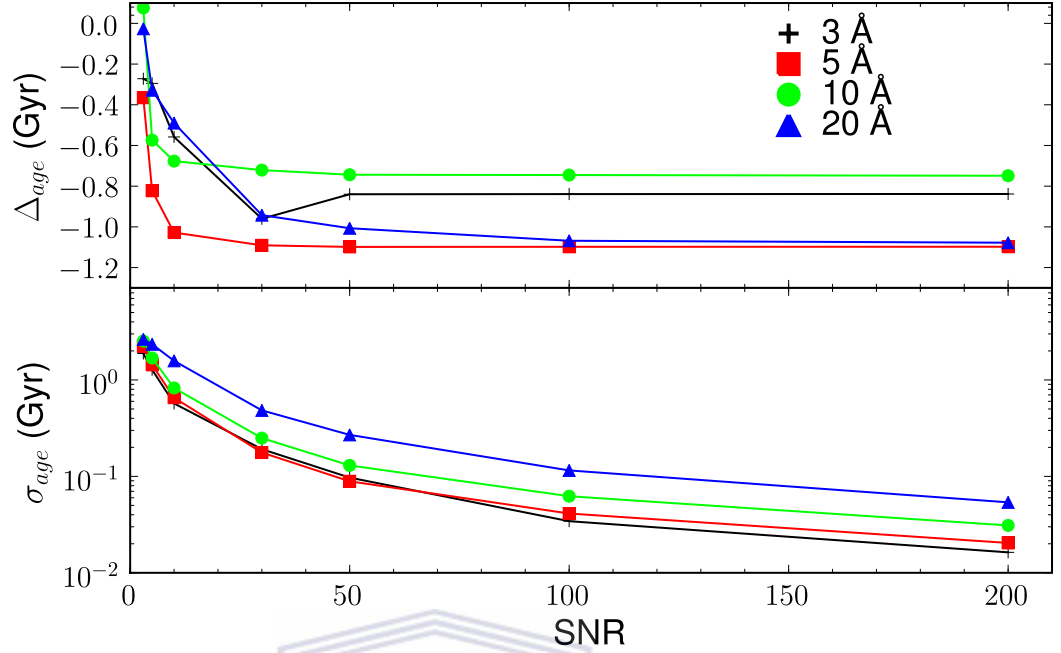


Figure 16: The average systematic offset between the model age and the mass-weighted age as a function of SNR and resolution for 10 different galaxies (Top panel). Random error in the age determination for the same 10 galaxies (bottom panel).

galaxy, this process was repeated 1000 times. Figure 16 demonstrates the variation of the difference between the minimum and maximum values of the systematic and random errors with the SNR depending on the spectral resolution. A typical result of these simulations is at a value of $SNR = 100$ and $\Delta\lambda = 5 \text{ \AA}$, the minimum and maximum values of the systematic and random errors for the 10 galaxies are $\Delta_{age} = 0.148 - 1.23 \text{ Gyr}$ and $\sigma_{age} = 0.025 - 0.045 \text{ Gyr}$.

There is some improvement with increasing SNR in this method even when using SSPs, in addition the same age at high SNR for all resolutions is potentially reproduced using this method. The random error on the age does decrease for smaller resolutions allowing for a better determination of the age. However, the poor accuracy of SSPs is again demonstrated in figure 16. The average systematic offset between the model and the mass-weighted age seems to settle at a given value at $SNR > 30$, but it does not seem to be a monotonic function of the spectral resolution.

6.4 Age-dating simulated LRG spectra with model spectra

Since the age-dating of LRGs with SSPs is not accurate enough for calculating $H(z)$, we investigate age-dating the simulated LRG spectra with composite spectra. The large model library of different LRGs that we have created provides mass-weighted ages and many spectra. We are therefore able to use these spectra as our templates instead of the SSP templates. To test this, we extracted one spectrum from the models and then used the remaining spectra to age-date this spectrum. We repeated that process for all other spectra. For each spectrum, we used its mass-weighted age as its fiducial age. In table 8, for our entire sample at the four redshifts, we show the results of the systematic and random errors in ages of the age-dating using the model spectra. As an example of the typical error in ages of the simulated LRG spectra at $z = 0.51$, we obtain a difference between the mass-weighted age and the measured age of $\Delta^b = -0.02Gyr$ and with a dispersion of $\sigma^c = 0.32$ ⁴. We can see clearly that the systematic error and dispersion error in ages have been reduced as compared to using SSPs. Thus these ages can be used to measure $H(z)$ because they have very small, regular bias with respect to the age of the Universe.

6.5 Summary

The LRG spectra were generated using BC03 models and the given SFH of galaxies; we then investigated the best method to age-date the LRG spectra. SSPs were not sufficient to accurately recover the ages of the individual galaxies as has been found recently by Maraston et al. (2009) and Trager and Somerville (2009). The accuracy of the age-dating is clearly critical for calculating $H(z)$. Unless systematic biases are constant with redshift and can be subtracted out or are well behaved and can be removed with modelling, they will contribute a significant systematic error to the age calculation. Even in this study of using model galaxies from the MS, the SSPs are not able to reproduce the age without significant bias and are thus not adequate for the

⁴Here Δ^b means the mean difference between measured age and mass-weighted age; and σ^c means the standard deviation of difference between measured age and mass-weighted age.

cosmic chronometer method. However, if we used the average star formation history from the MS, we are able to replicate the properties of the model spectra; and the obtained ages can be used to measure $H(z)$.



Chapter 7

7 Observation constraints



In this chapter, we explore the minimum observing time required to recover $H(z)$ to a precision of 3, 5 and 10% at $z \approx 0.42$. Table 8 indicates that the systematic error on individual ages of galaxies could be less than $0.3Gyr$ if suitable templates can be used. However, since it is still unclear what the uncertainty on individual ages of galaxies is in a realistic experiment, we explore observing requirements for four values of this uncertainty (0.05, 0.5, 1, $2Gyr$). We consider observations at two redshifts: $z = 0.32$ and $z = 0.51$, giving a redshift interval of $\Delta z = 0.19$. To simplify our estimate, the mean ages at the two redshifts are calculated using the average age of LRGs at each redshift (the first method in chapter 5). According to equation 43, the uncertainty on the mean ages will have to be $\sigma_{\langle age \rangle} = 0.03, 0.05, 0.10$ to measure $H(z)$ with 3, 5, 10% precision.

To estimate the uncertainty in the mean age as a function of the number of galaxies and the uncertainty on individual ages, we ran a Monte Carlo simulation. We assume the uncertainty on individual galaxy ages are normally distributed, and the galaxy ages are drawn from the probability distribution for galaxies at $z = 0.51$ given by fitting the normalized age distribution to equation 45. For each N , the simulation is repeated 1000 times and the standard deviation in the mean age is calculated. The results are presented in figure 17 and are used to calculate the total number of galaxies required to reach our desired precision.

The other constraint on the total observing time is the exposure time per galaxy. We assume that we are only able to measure one galaxy at a time but note that multi-object spectroscopy could be used. Figure 16 presents the SNR for different spectral resolutions. Even though the results in figure 16 are obtained using SSP fitting, we use them to provide a crude estimate of the resolution and SNR required to derive the random error on the ages of individual galaxies. From there, we use the SALT exposure time calculator for the Robert Stobie Spectrograph (RSS) (Kobulnicky et al., 2003) to calculate the exposure time required for an individual galaxy. We assume that our galaxies have rest-frame magnitudes of $M_V = -23$, which corresponds to $V = 19.56, 20.75$ at $z = 0.32, 0.51$ respectively. For our purposes we use the PG1300 VPH grating, which provides a resolution of $\Delta\lambda = 3 \text{ \AA}$. In figure 18, we combine all of

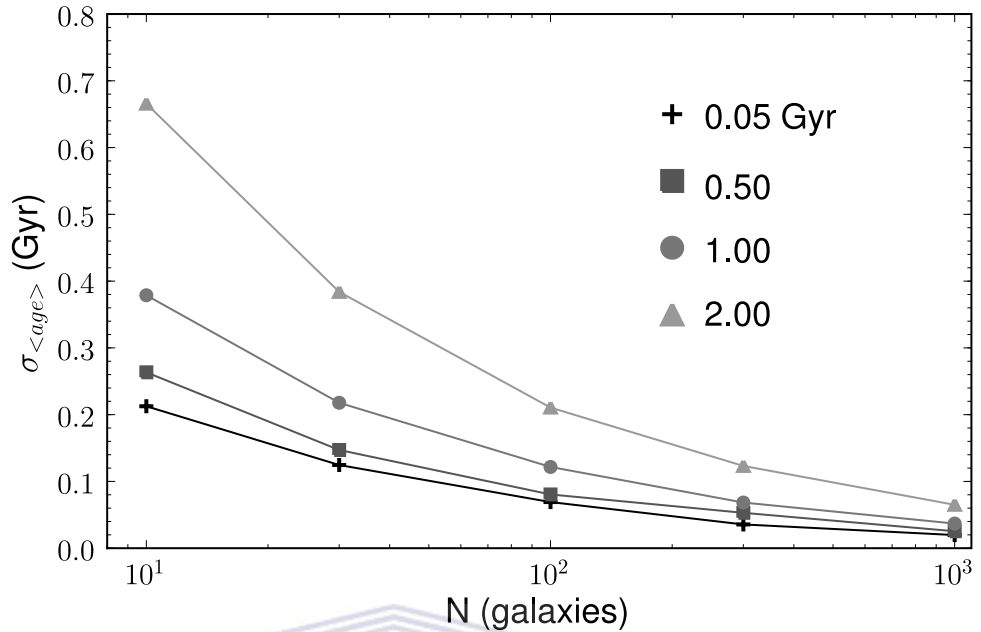


Figure 17: The uncertainty in the mean age of LRGs at $z = 0.51$ as a function of the number of galaxies used for the measurement. We assumed four different uncertainties (0.05, 0.50, 1, 2 Gyr) in the measured age of an individual galaxy in sample

this information to calculate the total time needed as a function of signal to noise to measure $H(z)$ to a precision of 3, 5 and 10%. In these calculations, we have assumed an overhead time of 300s per observation. The minimum total time required for the observations for $H(z) = 3, 5, 10\%$ would be $T = 184, 72, 17$ hours respectively. In total we need to observe 840, 327, 80 galaxies at each redshift in order to achieve this accuracy. A $SNR = 11$, where the minimum occurs in the total time, corresponds to approximately an exposure time of 95s with SALT and an individual error on each galaxy of $\sigma_{age} = 0.5 Gyr$.

In our estimate of the total observing time required, we have made a number of assumptions about the observations of LRGs. We have based our estimate of σ_{age} on the results of the simulations in chapter 6 section 3 and those results are likely a best-case scenario. However, the observing time per galaxy is still relatively small especially compared to the overhead. We have not considered issues affecting systematic errors

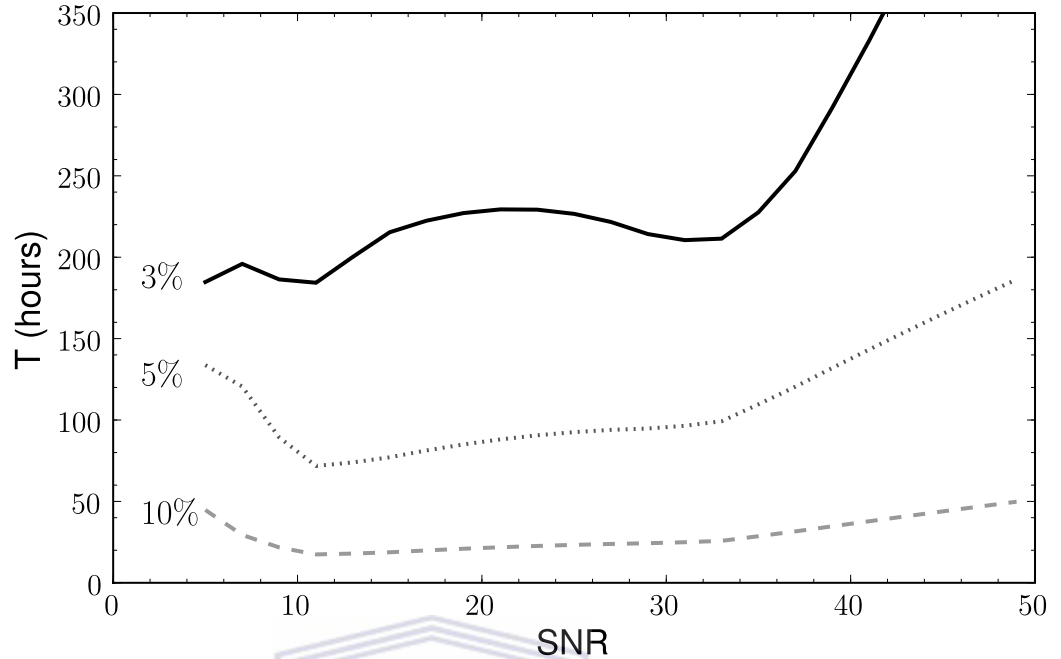


Figure 18: The total observing time required with SALT to measure $H(z)$ at $z \approx 0.415$ to 3, 5 and 10% as a function of SNR of the observations. All observations are for $\Delta\lambda = 3 \text{ \AA}$ and an overhead of 300 s per observation.

on the total observing time, but save that for future work. If we must increase the SNR for individual galaxies to minimize systematic effects, an increase by a factor of 3 in the required SNR would not result in a significant increase in the total observing time due to the smaller number of galaxies that would be required. Above about $SNR = 30$, the total observing time begins to increase rapidly as seen in figure 18.

We have also not included how well we could parameterize $H(z)$ based on measurements at multiple redshifts. RSS can be used in multi-object mode and up to 50 spectra could be obtained at one time over the $8 \times 8'$ field of view. Depending on the clustering, several LRGs may be expected in each field of view based on the space density of the objects. Using the absolute magnitude cuts, we estimate this to be $3.5 \times 10^{-5} \text{ Mpc}^{-3}$ from the SDSS (without considering the effects of incompleteness), which is comparable to the value from MS even if it is slightly low. If we are able to observe two additional LRGs per set-up with $z = 0.1 - 0.6$ while calculating $H(z)$ to

3%, as outlined above to 10% at redshifts between $z = 0.1 - 0.6$. This would put a far tighter constraint on the value of $H(z)$ than measuring it from two redshift bins alone.



Chapter 8

8 Summary and Conclusion



The work presented in this thesis explores the idea that Luminous Red Galaxies with observed SALT can be used to measure the expansion rate of the Universe at $z \approx 0.5$. We have highlighted a number of assumptions throughout this work. Through analysis of the Millenium Simulation LRGs and the use of stellar population models, we conclude that LRGs, when selected by the appropriate selection criteria, can be used as cosmic chronometers within the simulation. Generally, the star formation histories of LRGs are not completely homogeneous as assumed by [Jimenez and Loeb \(2002\)](#). Only the de Lucia et al. model has given us a single age of LRGs with a tail of young populations. $H(z)$ can still be calculated to an accuracy better than 3%. However using SSPs was not sufficient to accurately recover the ages of individual galaxies and it was only when we used our model spectra that we were able to recover ages with sufficient accuracy.

8.1 Summary

In the first part of this thesis, I summarized the difference between the semi-analytic models for galaxy evolution given by de Lucia et al. (2006) and Bower et al. (2006). We explored which selection criteria and model provided the number of homogeneous Luminous Red Galaxies which we think could be used to measure the expansion rate of the Universe at $z \approx 0.5$ using SALT. During this analysis, we showed that selecting LRGs using SDSS criteria in both the de Lucia et al. and Bower et al. models does not produce the large sample of LRGs with similar SFHs required for age-dating. Note that this SDSS selection criteria by [Eisenstein \(2001\)](#) is based on the apparent magnitude cuts. By selecting the galaxies with their rest-frame properties, we find that we can create a more homogeneous sample of objects. In the de Lucia et al. model, for galaxies at $z \sim 0.3 - 0.6$, we find that cuts of $M_V < -23$ and $B - V > 0.81$ select a sample of galaxies with similar star formation histories and formation redshifts (figure 5). However in the Bower et al. model, even though similar cuts have been used, more galaxies have recent bursts (figure 8). There are few red and bright galaxies in this model looking at the galaxy color-diagram. We thus decided to continue the analysis

with the sample of galaxies in the de Lucia et al. model. Therefore, the galaxies in our final sample do show very similar star formation histories with very little star formation since $z \sim 1.7$. The ages also show the 'downsizing effect' (Cowie et al., 1996) where the oldest galaxies are in the most massive haloes. The distributions of the ages are very similar with each showing a small tail towards younger ages, but with a very strong peak at a single age.

The homogeneity of galaxies in the de Lucia et al. model suggests that these galaxies can be used as cosmic chronometers. To test this we have used three different methods to measure $H(z)$ and to explore the uncertainties on $H(z)$. The methods consist of calculating the average ages, calculating a fit to a distribution, and comparing the ages of pairs of galaxies. All of these methods were indeed able to recover the cosmology used in the de Lucia et al. model. Using only galaxies selected from two redshifts, we find that we are able to calculate $H(z)$, implied by the cosmological parameters of the simulation, to a precision of less than 3%.

Using the Bruzual and Charlot 2003 model, we produced LRG spectra for four different redshifts. We showed that using SSPs was not sufficient to accurately recover the ages for individual galaxies, which is not a surprise according to the results given by other samples (e.g Maraston et al., 2009; Trager and Somerville, 2009). Regardless of the relatively simple nature of the SFHs in the de Lucia et al. model in figure 5, the calculated SSP ages were dominated by the most recent burst of star formation. We conclude that if we use the average star formation history of galaxies from the MS, we are able to age-date the galaxies well enough.

We estimated the required time for the experiment using the Robert Stobie Spectrograph (RSS) on SALT. We need in total ~ 180 hours which includes observing overheads to calculate $H(z)$ at $z \approx 0.42$ to 3% assuming the age uncertainties well controlled. With these observations, it is probable that tighter constraints could be obtained using multi-object spectroscopy on the evolution of $H(z)$.

8.2 Outlook

We will investigate age-dating of LRGs in more detail by determining which part of the spectrum is the most sensitive, and by exploring different age-dating techniques (e.g. full spectrum versus lick indices, etc.). We plan to carry out the observation of LRGs described here in 2010. Apart from constraining $H(z)$, the data will provide us with a great deal of information on the evolution of the most massive galaxies at intermediate redshift.



References

- Abazajian, K. N., *et al.* : 2009, *Astrophysical Journal, Supplement* **182**, 543
- Almeida, C., Baugh, C. M., Wake, D. A., Lacey, C. G., Benson, A. J., Bower, R. G., and Pimblett, K.: 2008, *Monthly Notices of the Royal Astronomical Society* **386**, 2145
- Avila-Reese, V., Firmani, C., and Hernández, X.: 1998, *Astrophysical Journal* **505**, 37
- Barber, T., Meiksin, A., and Murphy, T.: 2007, *Monthly Notices of the Royal Astronomical Society* **377**, 787
- Baugh, C. M.: 2006, *Astronomy and Geophysics* **47(2)**, 020000
- Baugh, C. M., Cole, S., and Frenk, C. S.: 1996, *Monthly Notices of the Royal Astronomical Society* **282**, L27
- Baugh, J., Moussa, O., Ryan, C. A., Nayak, A., and Laflamme, R.: 2005, *Nature* **438**, 470
- Benoît, A., *et al.* : 2003, *Astronomy and Astrophysics* **399**, L19
- Benson, A. J., Kamionkowski, M., and Hassani, S. H.: 2005, *Monthly Notices of the Royal Astronomical Society* **357**, 847
- Bernardi, M., Nichol, R. C., Sheth, R. K., Miller, C. J., and Brinkmann, J.: 2006, *Astronomical Journal* **131**, 1288
- Bertone, E., Buzzoni, A., Chávez, M., and Rodríguez-Merino, L. H.: 2008, *Astronomy and Astrophysics* **485**, 823
- Binney, J. and Tremaine, S.: 1987, *Galactic dynamics, Princeton University Press, 1987, 747 p.*
- Blake, C., Collister, A., and Lahav, O.: 2008, *Monthly Notices of the Royal Astronomical Society* **385**, 1257

- Blanton, E. L., Gregg, M. D., Helfand, D. J., Becker, R. H., and White, R. L.: 2000, *Astrophysical Journal* **531**, 118
- Blanton, M. R., Eisenstein, D. J., Hogg, D. W., Schlegel, D. J. S., Brinkmann, J., Quintero, A. D., Berlind, A., and Wherry, N.: 2003, in *Bulletin of the American Astronomical Society*, Vol. 36 of *Bulletin of the American Astronomical Society*, pp 589–+
- Bower, R. G., Benson, A. J., Malbon, R., Helly, J. C., Frenk, C. S., Baugh, C. M., Cole, S., and Lacey, C. G.: 2006, *Monthly Notices of the Royal Astronomical Society* **370**, 645
- Bower, R. G., Ellis, R. S., Rose, J. A., and Sharples, R. M.: 1990, *Astronomical Journal* **99**, 530
- Bower, R. G., Lucey, J. R., and Ellis, R. S.: 1992, *Monthly Notices of the Royal Astronomical Society* **254**, 601
- Bruzual, G. and Charlot, S.: 2003, *Monthly Notices of the Royal Astronomical Society* **344**, 1000
- Cabr e, A. and Gazta naga, E.: 2009, *Monthly Notices of the Royal Astronomical Society* **396**, 1119
- Capozziello, S., Cardone, V. F., Funaro, M., and Andreon, S.: 2004, *Physical Review D* **70(12)**, 123501
- Chabrier, G.: 2003, *Astrophysical Journal, Letters* **586**, L133
- Cole, S., Aragon-Salamanca, A., Frenk, C. S., Navarro, J. F., and Zepf, S. E.: 1994, *Monthly Notices of the Royal Astronomical Society* **271**, 781
- Cole, S., Lacey, C. G., Baugh, C. M., and Frenk, C. S.: 2000, *Monthly Notices of the Royal Astronomical Society* **319**, 168

- Colless, M., *et al.* : 2001, *Monthly Notices of the Royal Astronomical Society* **328**, 1039
- Colless, M., Peterson, B. A., Jackson, C., Peacock, J. A., Cole, S., Norberg, P., Baldry, I. K., Baugh, C. M., Bland-Hawthorn, J., Bridges, T., Cannon, R., Collins, C., Couch, W., Cross, N., Dalton, G., De Propris, R., Driver, S. P., Efstathiou, G., Ellis, R. S., Frenk, C. S., Glazebrook, K., Lahav, O., Lewis, I., Lumsden, S., Maddox, S., Madgwick, D., Sutherland, W., and Taylor, K.: 2003, *arXiv:astro-ph/0306581*
- Conroy, C., Gunn, J. E., and White, M.: 2009, *Astrophysical Journal* **699**, 486
- Conroy, C., Ho, S., and White, M.: 2007, *Monthly Notices of the Royal Astronomical Society* **379**, 1491
- Cowie, L. L., Songaila, A., Hu, E. M., and Cohen, J. G.: 1996, *Astronomical Journal* **112**, 839
- Croton, D. J., Springel, V., White, S. D. M., De Lucia, G., Frenk, C. S., Gao, L., Jenkins, A., Kauffmann, G., Navarro, J. F., and Yoshida, N.: 2006, *Monthly Notices of the Royal Astronomical Society* **365**, 11
- Dantas, M. A., Alcaniz, J. S., Jain, D., and Dev, A.: 2007, *Astronomy and Astrophysics* **467**, 421
- Davé, R.: 2008, *Monthly Notices of the Royal Astronomical Society* **385**, 147
- Davis, M., Efstathiou, G., Frenk, C. S., and White, S. D. M.: 1985, *Astrophysical Journal* **292**, 371
- De Lucia, G. and Blaizot, J.: 2007, *Monthly Notices of the Royal Astronomical Society* **375**, 2
- De Lucia, G., Springel, V., White, S. D. M., Croton, D., and Kauffmann, G.: 2006, *Monthly Notices of the Royal Astronomical Society* **366**, 499

- Efstathiou, G., *et al.* : 2002, *Monthly Notices of the Royal Astronomical Society* **330**, L29
- Eisenstein, D. J., *et al.* : 2001, *Astronomical Journal* **122**, 2267
- Eisenstein, D. J., *et al.* : 2005, *Astrophysical Journal* **633**, 560
- Eisenstein, D. J., Hogg, D. W., Fukugita, M., Nakamura, O., Bernardi, M., Finkbeiner, D. P., Schlegel, D. J., Brinkmann, J., Connolly, A. J., Csabai, I., Gunn, J. E., Ivezić, Ž., Lamb, D. Q., Loveday, J., Munn, J. A., Nichol, R. C., Schneider, D. P., Strauss, M. A., Szalay, A., and York, D. G.: 2003, *Astrophysical Journal* **585**, 694
- Eke, V. R., *et al.* : 2004, *Monthly Notices of the Royal Astronomical Society* **355**, 769
- Evrard, A. E., Summers, F. J., and Davis, M.: 1994, *Astrophysical Journal* **422**, 11
- Faber, S. M., *et al.* : 2007, *Astrophysical Journal* **665**, 265
- Faber, S. M.: 1973, *Astrophysical Journal* **179**, 731
- Fardal, M. A., Katz, N., Weinberg, D. H., and Davé, R.: 2007, *Monthly Notices of the Royal Astronomical Society* **379**, 985
- Ferrarese, L. and Merritt, D.: 2000, *Astrophysical Journal, Letters* **539**, L9
- Ferreras, I., Melchiorri, A., and Silk, J.: 2001, *Monthly Notices of the Royal Astronomical Society* **327**, L47
- Ferreras, I., Melchiorri, A., and Tocchini-Valentini, D.: 2003, *Monthly Notices of the Royal Astronomical Society* **344**, 257
- Fioc, M. and Rocca-Volmerange, B.: 1997, *Astronomy and Astrophysics* **326**, 950
- Freedman, W. L., Madore, B. F., Gibson, B. K., Ferrarese, L., Kelson, D. D., Sakai, S., Mould, J. R., Kennicutt, Jr., R. C., Ford, H. C., Graham, J. A., Huchra, J. P., Hughes, S. M. G., Illingworth, G. D., Macri, L. M., and Stetson, P. B.: 2001, *Astrophysical Journal* **553**, 47

- Frenk, C. S., Evrard, A. E., White, S. D. M., and Summers, F. J.: 1996, *Astrophysical Journal* **472**, 460
- Frenk, C. S., White, S. D. M., Bode, P., Bond, J. R., Bryan, G. L., Cen, R., Couchman, H. M. P., Evrard, A. E., Gnedin, N., Jenkins, A., Khokhlov, A. M., Klypin, A., Navarro, J. F., Norman, M. L., Ostriker, J. P., Owen, J. M., Pearce, F. R., Pen, U., Steinmetz, M., Thomas, P. A., Villumsen, J. V., Wadsley, J. W., Warren, M. S., Xu, G., and Yepes, G.: 1999, *Astrophysical Journal* **525**, 554
- Fukugita, M., Ichikawa, T., Gunn, J. E., Doi, M., Shimasaku, K., and Schneider, D. P.: 1996, *Astronomical Journal* **111**, 1748
- Gallazzi, A., Charlot, S., Brinchmann, J., and White, S. D. M.: 2006, *Monthly Notices of the Royal Astronomical Society* **370**, 1106
- Gallazzi, A., Charlot, S., Brinchmann, J., White, S. D. M., and Tremonti, C. A.: 2005, *Monthly Notices of the Royal Astronomical Society* **362**, 41
- Gaztañaga, E., Cabré, A., Castander, F., Crocce, M., and Fosalba, P.: 2009, *Monthly Notices of the Royal Astronomical Society* pp 1149–+
- Gunn, J. E., *et al.* : 2006, *Astronomical Journal* **131**, 2332
- Heyl, J. S., Cole, S., Frenk, C. S., and Navarro, J. F.: 1995, *Monthly Notices of the Royal Astronomical Society* **274**, 755
- Hodge, J. A., Zeimann, G. R., Becker, R. H., and White, R. L.: 2009, *Astronomical Journal* **138**, 900
- Hogg, D. W., *et al.* : 2002, *Astronomical Journal* **124**, 646
- Hubble, E.: 1936, *Astrophysical Journal* **84**, 158
- Jimenez, R. and Haiman, Z.: 2006, *Nature* **440**, 501
- Jimenez, R. and Loeb, A.: 2002, *Astrophysical Journal* **573**, 37

- Jimenez, R., MacDonald, J., Dunlop, J. S., Padoan, P., and Peacock, J. A.: 2004, *Monthly Notices of the Royal Astronomical Society* **349**, 240
- Jimenez, R., Verde, L., Treu, T., and Stern, D.: 2003, *Astrophysical Journal* **593**, 622
- Kannappan, S. J. and Gawiser, E.: 2007, *Astrophysical Journal, Letters* **657**, L5
- Katz, N., Hernquist, L., and Weinberg, D. H.: 1992, *Astrophysical Journal, Letters* **399**, L109
- Kauffmann, G.: 1996, *Monthly Notices of the Royal Astronomical Society* **281**, 475
- Kauffmann, G. and Charlot, S.: 1998, *ArXiv Astrophysics e-prints*
- Kauffmann, G., Charlot, S., and Haehnelt, M.: 2000, in *Astronomy, physics and chemistry of H_3^+* , Vol. 358 of *Royal Society of London Philosophical Transactions Series A*, pp 2121–+
- Kauffmann, G., Nusser, A., and Steinmetz, M.: 1997, *Monthly Notices of the Royal Astronomical Society* **286**, 795
- Kauffmann, G. and White, S. D. M.: 1993, *Monthly Notices of the Royal Astronomical Society* **261**, 921
- Kennicutt, R., Moss, C., Sakai, S., and Whittle, M.: 1999, in *NOAO Proposal ID #1999A-0240*, pp 240–+
- Kennicutt, Jr., R. C.: 1983, *Astrophysical Journal* **272**, 54
- Kereš, D., Katz, N., Weinberg, D. H., and Davé, R.: 2005, *Monthly Notices of the Royal Astronomical Society* **363**, 2
- Kobulnicky, H. A., Nordsieck, K. H., Burgh, E. B., Smith, M. P., Percival, J. W., Williams, T. B., and O'Donoghue, D.: 2003, in M. Iye & A. F. M. Moorwood (ed.), *Society of Photo-Optical Instrumentation Engineers (SPIE) Conference Series*, Vol. 4841 of *Society of Photo-Optical Instrumentation Engineers (SPIE) Conference Series*, pp 1634–1644

- Kroupa, P.: 2001, *Monthly Notices of the Royal Astronomical Society* **322**, 231
- Lacey, C. and Cole, S.: 1993, *Monthly Notices of the Royal Astronomical Society* **262**, 627
- Lacey, C. and Silk, J.: 1991, *Astrophysical Journal* **381**, 14
- Le Borgne, J., Bruzual, G., Pelló, R., Lançon, A., Rocca-Volmerange, B., Sanahuja, B., Schaerer, D., Soubiran, C., and Vílchez-Gómez, R.: 2003, *Astronomy and Astrophysics* **402**, 433
- Lemson, G. and Springel, V.: 2006, in C. Gabriel, C. Arviset, D. Ponz, & S. Enrique (ed.), *Astronomical Data Analysis Software and Systems XV*, Vol. 351 of *Astronomical Society of the Pacific Conference Series*, pp 212–+
- Lemson, G. and Virgo Consortium, t.: 2006, *ArXiv Astrophysics e-prints*
- Longhetti, M. and Saracco, P.: 2009, *Monthly Notices of the Royal Astronomical Society* **394**, 774
- Malbon, R. K., Baugh, C. M., Frenk, C. S., and Lacey, C. G.: 2007, *Monthly Notices of the Royal Astronomical Society* **382**, 1394
- Maraston, C.: 2005, *Monthly Notices of the Royal Astronomical Society* **362**, 799
- Maraston, C., Strömbäck, G., Thomas, D., Wake, D. A., and Nichol, R. C.: 2009, *Monthly Notices of the Royal Astronomical Society* **394**, L107
- Marigo, P., Girardi, L., Bressan, A., Groenewegen, M. A. T., Silva, L., and Granato, G. L.: 2008, *Astronomy and Astrophysics* **482**, 883
- Masjedi, M., Hogg, D. W., Cool, R. J., Eisenstein, D. J., Blanton, M. R., Zehavi, I., Berlind, A. A., Bell, E. F., Schneider, D. P., Warren, M. S., and Brinkmann, J.: 2006, *Astrophysical Journal* **644**, 54

- Mo, H. J. and Mao, S.: 2000, in F. Combes, G. A. Mamon, & V. Charmandaris (ed.), *Dynamics of Galaxies: from the Early Universe to the Present*, Vol. 197 of *Astronomical Society of the Pacific Conference Series*, pp 145–+
- Mo, H. J., Mao, S., and White, S. D. M.: 1998, *Monthly Notices of the Royal Astronomical Society* **295**, 319
- Mo, H. J., Mao, S., and White, S. D. M.: 1999, *Monthly Notices of the Royal Astronomical Society* **304**, 175
- Muzzin, A., Marchesini, D., van Dokkum, P. G., Labbé, I., Kriek, M., and Franx, M.: 2009, *Astrophysical Journal* **701**, 1839
- Navarro, J. F.: 1995, *ArXiv Astrophysics e-prints*
- Navarro, J. F., Frenk, C. S., and White, S. D. M.: 1997, *Astrophysical Journal* **490**, 493
- Padmanabhan, N., *et al.* : 2007, *Monthly Notices of the Royal Astronomical Society* **378**, 852
- Pearce, F. R., Jenkins, A., Frenk, C. S., Colberg, J. M., White, S. D. M., Thomas, P. A., Couchman, H. M. P., Peacock, J. A., Efstathiou, G., and The Virgo Consortium: 1999, *Astrophysical Journal, Letters* **521**, L99
- Perlmutter, S., *et al.* : 1999, *Astrophysical Journal* **517**, 565
- Roseboom, I. G., *et al.* : 2006, *Monthly Notices of the Royal Astronomical Society* **373**, 349
- Ross, N. P., Shanks, T., Cannon, R. D., Wake, D. A., Sharp, R. G., Croom, S. M., and Peacock, J. A.: 2008, *Monthly Notices of the Royal Astronomical Society* **387**, 1323
- Ross, N. P., Shanks, T., and Cruz da Ângela, J.: 2007, in N. Metcalfe & T. Shanks (ed.), *Cosmic Frontiers*, Vol. 379 of *Astronomical Society of the Pacific Conference Series*, pp 68–+

- Sakharov, A. S. and Hofer, H.: 2003, *ArXiv Astrophysics e-prints*
- Samushia, L., Dev, A., Jain, D., and Ratra, B.: 2009, *ArXiv e-prints:0906.2734*
- Sanchez, A. G., Crocce, M., Cabre, A., Baugh, C. M., and Gaztanaga, E.: 2009, *ArXiv e-prints:0901.2570*
- Simien, F. and de Vaucouleurs, G.: 1986, *Astrophysical Journal* **302**, 564
- Simon, J., Verde, L., and Jimenez, R.: 2005, *Physical Review D* **71(12)**, 123001
- Somerville, R. S. and Primack, J. R.: 1999, *Monthly Notices of the Royal Astronomical Society* **310**, 1087
- Spergel, D. N., Verde, L., Peiris, H. V., Komatsu, E., Nolta, M. R., Bennett, C. L., Halpern, M., Hinshaw, G., Jarosik, N., Kogut, A., Limon, M., Meyer, S. S., Page, L., Tucker, G. S., Weiland, J. L., Wollack, E., and Wright, E. L.: 2003, *Astrophysical Journal, Supplement* **148**, 175
- Spinrad, H., Dey, A., Stern, D., Dunlop, J., Peacock, J., Jimenez, R., and Windhorst, R.: 1997, *Astrophysical Journal* **484**, 581
- Springel, V., White, S. D. M., Jenkins, A., Frenk, C. S., Yoshida, N., Gao, L., Navarro, J., Thacker, R., Croton, D., Helly, J., Peacock, J. A., Cole, S., Thomas, P., Couchman, H., Evrard, A., Colberg, J., and Pearce, F.: 2005, *Nature* **435**, 629
- Springel, V., Yoshida, N., and White, S. D. M.: 2001, *New Astronomy* **6**, 79
- Strateva, I., *et al.* : 2001, *Astronomical Journal* **122**, 1861
- Thomas, D., Maraston, C., Bender, R., and Mendes de Oliveira, C.: 2005, *Astrophysical Journal* **621**, 673
- Thomas, D., Maraston, C., and Korn, A.: 2004, *Monthly Notices of the Royal Astronomical Society* **351**, L19

- Trager, S. C., Faber, S. M., Worthey, G., and González, J. J.: 2000, *Astronomical Journal* **119**, 1645
- Trager, S. C. and Somerville, R. S.: 2009, *Monthly Notices of the Royal Astronomical Society* **395**, 608
- van Dokkum, P. G.: 2008, *Astrophysical Journal* **674**, 29
- van Kampen, E., Jimenez, R., and Peacock, J. A.: 1999, *Monthly Notices of the Royal Astronomical Society* **310**, 43
- Verkhodanov, O. V., Parijskij, Y. N., and Starobinsky, A. A.: 2005, *Bull. Special Astrophys. Obs.* **58**, 5
- Visvanathan, N. and Sandage, A.: 1977, *Astrophysical Journal* **216**, 214
- Wake, D. A., *et al.* : 2006, *Monthly Notices of the Royal Astronomical Society* **372**, 537
- Walcher, C. J. *et al.* : 2008, *Astronomy and Astrophysics* **491**, 713
- Walcher, C. J., Coelho, P., Gallazzi, A., and Charlot, S.: 2009, *Monthly Notices of the Royal Astronomical Society* **398**, L44
- Wang, X., Tegmark, M., Jain, B., and Zaldarriaga, M.: 2003, *Physical Review D* **68(12)**, 123001
- Watson, D. and Berlind, A.: 2009, in *Bulletin of the American Astronomical Society*, Vol. 41 of *Bulletin of the American Astronomical Society*, pp 335–+
- White, S. D. M. and Frenk, C. S.: 1991, *Astrophysical Journal* **379**, 52
- White, S. D. M. and Rees, M. J.: 1978, *Monthly Notices of the Royal Astronomical Society* **183**, 341
- Wolf, M. J., Drory, N., Gebhardt, K., and Hill, G. J.: 2007, *Astrophysical Journal* **655**, 179

- Yan, L., McCarthy, P. J., Freudling, W., Teplitz, H. I., Malumuth, E. M., Weymann, R. J., and Malkan, M. A.: 1999, *Astrophysical Journal, Letters* **519**, L47
- York, D. G., *et al.* : 2000, *Astronomical Journal* **120**, 1579
- Zehavi, I., Eisenstein, D. J., Nichol, R. C., Blanton, M. R., Hogg, D. W., Brinkmann, J., Loveday, J., Meiksin, A., Schneider, D. P., and Tegmark, M.: 2005, *Astrophysical Journal* **621**, 22
- Zheng, Z., Zehavi, I., Eisenstein, D. J., Weinberg, D. H., and Jing, Y.: 2008, *ArXiv e-prints:0809.1868*
- Zwicky, F.: 1933, *Helvetica Physica Acta* **6**, 110

